TAMPEREEN TEKNILLINEN YLIOPISTO
TAMPERE UNIVERSITY OF TECHNOLOGY

MARLITT VIEHRIG

TRANSPARENT ELECTROMECHANICAL STIMULATION SYSTEM FOR STEM CELL APPLICATIONS

Master of Science Thesis

Examiners: Prof. Pasi Kallio
Asst. Prof. Sampo Tuukkanen

Examiners and topic approved by the
Faculty Council of Natural Sciences
on 3rd February 2016

ABSTRACT

MARLITT VIEHRIG: Transparent Electromechanical Stimulation System for Stem Cell Applications
Tampere University of Technology
Master of Science Thesis, 72 pages, 2 Appendix pages
May 2016
Master's Degree Programme in Science and Bioengineering
Major: Biomeasurements
Examiners: Professor Pasi Kallio
Assistant Professor Sampo Tuukkanen

Keywords: Electromechanical Stimulation, Stem Cells, Conductive Polymers, Piezoelectricity, Innophene, Cellulose Nanocrystals, PDMS, Stretchable Electrodes

Functionalities of cells and tissues in the human body depend greatly on their specific microenvironment created by a variety of biochemical, electrical and mechanical cues. Current standard *in vitro* cell cultivation technologies fail to mimic the cellular microenvironment in its full complexity, which makes them unsuitable as physiological models for example in drug development. Therefore, the development of a controlled, biomimetic cell cultivation technology that combines and recreates all features of the cellular microenvironment is of high importance especially in stem cell research.

This study introduces two optional system design approaches for a transparent electromechanical cell stimulation device usable for *in vitro* cell stimulation. The device is aimed as a modular expansion of an earlier introduced mechanical cell stimulation platform. Hereby, it is of high importance that the new electrical-stimulative module expands the functionalities of the existing device, without affecting its original capabilities and benefits. This is realized through incorporation of a stretchable, transparent, electrical-stimulative component in the existing system. The first approach focuses on direct electrical stimulation of cells through transparent conductive polymers, which allows flexible electrical stimulation independent from mechanical stimulation. In the second approach, a system design that utilizes indirect electrical stimulation coupled to the mechanical stimulus created by an embedded piezoelectric layer of cellulose nanocrystals is studied.

Various structural integration strategies for the fabrication of stretchable conductive electrodes and nanocomposites containing cellulose nanocrystals thin-films are presented. Their success is evaluated in regards to their structural properties, mechanical durability, electro-stimulative functionality as well as biocompatibility.

Stretchable conductive electrodes could only be introduced to the mechanical stimulation system in the form of channel casted electrodes, with limited equiaxial stretchability. However, the fabricated structures were highly transparent and expressed beneficial biological properties. The experimental work also resulted in a new technical approach to create thin, transparent nanocellulose composite, based on surface integration technologies. The achieved structure is easily integrable in the existing mechanical stimulation device, without limiting its transparency, stretchability or biocompatibility.

PREFACE

This thesis has been conducted at the Department of Automation Science and Engineering (ASE), Tampere University of Technology, Finland. It is a result of a collaborative effort by the Micro- and Nanosystems and Nanoscale Phenomena and Measurements research groups at the Department. The presented topic is based on results obtained during the Human Spare Parts Project I at the Institute for Biosciences and Medical Technology, in which I actively participated. Partial content of this thesis has been accepted as a full conference paper for the IEEE International Conference on Manipulation, Automation and Robotics at Small Scale, in which I am listed as first author.

First, I would like to thank my supervisors Pasi Kallio and Sampo Tuukkanen for the opportunity to pursue my own research visions under their funding. I am also grateful for their trust and ongoing scientific support during my work. I would also like to thank Joose Kreutzer for sharing his inventions and ideas with me as well as for fruitful discussions during the preparation of this thesis. In addition, I would like to thank Satu Rajala for conducting piezoelectric activity measurements on my samples, which are covered in this thesis, as well as Tiina Vuorinen and Matti Mäntysalo from the Department of Electronics and Communications Engineering at Tampere University of Technology for sharing their knowledge about printable electronics and conductive polymers.

I am thankful to ASE members Marika Janka, Antti-Juhana Mäki and Anne Skogberg for their expertise in electrical measurements and stimulation. Also, I wish to thank all members of the Micro- and Nanosystems group and ASE for creating an inspiring and pleasant work environment.

Most importantly, I wish to express my deepest gratitude and love for my parents Heike and Maik Viehrig, who never cease to compassionately support me in my life choices. Also my deepest thanks to my beloved partner Lukas Tietz for all his patience and love during the writing process. Finally, I would like to thank my friends for their support.

Tampere, 25.05.2016

Marlitt Viehrig

CONTENTS

LIST OF ABBREVIATIONS

2D	Two Dimensional
BioMEMS	Biomedical Microelectromechanical Systems
CNC	Cellulose Nanocrystals
CNF	Cellulose Nanofibrils
CNT	Carbon Nanotubes
DIC	Differential Interference Contrast
ECM	Extracellular Microenvironment
hiPSC	Human Induced Pluripotent Stem Cell
hiPSC-CM	Human Induced Pluripotent Stem Cell Derived Cardiomyocyte
IP	Innophene, Phene^{TM} Plus Series conductive polymer
MEF	Mouse Embryonic Fibroblasts
PBS	Phosphate Buffered Saline
PEDOT:PSS	Poly(3,4-ethylenedioxythiophene)-poly(styrene sulfonate)
PET	Polyethylene Terephthalate
PDMS	Polydimethylsiloxane
PH	Phase Contrast
PS	Polystyrene
PVDF	Polyvinylidene Fluoride
rpm	Rounds per Minute
UV	Ultraviolet
Vin	Vinculin

LIST OF SYMBOLS

A	area
c	concentration
D	diameter
d	thickness
d_{mn}	piezoelectric coefficient
ε_P	in-plane strain
F	force
h	height
l_n	specific landmark position
l	length
L_T	landmark distance
m	mass
w	width
w/w	mass fraction
x	horizontal position coordinate
y	vertical position coordinate

1. INTRODUCTION

Functionalities of cells and tissues in the human body greatly depend on biochemical, mechanical and electrical cues expressed by the cellular microenvironment [1-7]. This highly specific extracellular microenvironment (ECM) is largely responsible for cell maturation and functional fate [2-3] [5-6]. Standard *in vitro* cell cultivation technologies are merely able to recreate the biochemical cues present in the human body. Therefore, they fail to mimic the entirety of the ECM, which makes them unsuitable as physiologically relevant *in vivo* models [8]. Thus, the development of biomimetic cell cultivation devices that recreates complex cellular microenvironments is of high importance especially for stem cell research.

Mechanical cell stimulation platforms utilizing a variety of system approaches have been developed over the recent years [10-13]. However, such systems are often not compatible with standard single-cell analysis or optical microscopy procedures, as they are bulky or cannot withstand the high humidity conditions in a cell incubator. J. Kreutzer et. al [13] developed a modular mechanical stimulation platform for stem cell research, which enables controlled mechanical stimulation and is compatible with standard cell analysis procedures utilized in research. Mechanical strain is created via a partial vacuum pressure applied to a cavity in a two-shell system with an attached flexible membrane. The vacuum pressure causes the inner shell to buckle outwards causing an equiaxial in-plane strain of maximal 10 % to the membrane. Stem cells attached to the membrane through covalent functionalization experience a controlled equiaxial strain. Through a pressure control set-up various stretching modes can be realized, such as static and sinusoidal strains. Fig.1 shows the system and its functionality.

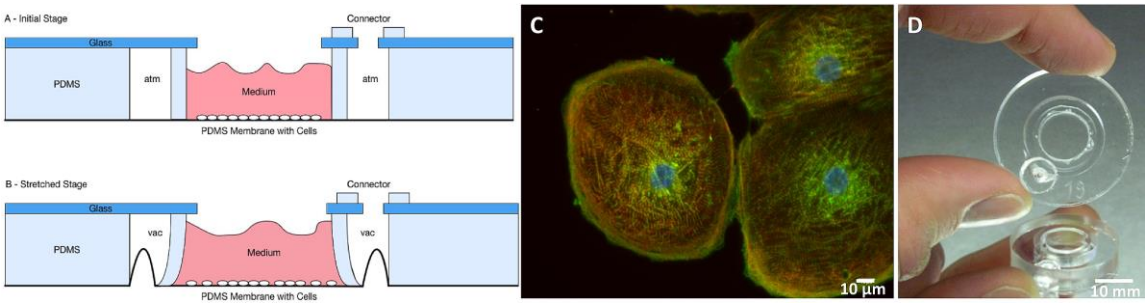

Figure 1. *Schematic working principle (A, B) and photograph (D) of the equiaxial pneumatic stretching device developed by J. Kreutzer et. al. Optical system capabilities are illustrated through a fluorescence image of human induced pluripotent stem cell (hiPSC) derived cardiomyocytes. (Adapted from* [13], [14]*)*

1.1 Scope of the Thesis

The aim of this case study is to introduce a flexible, transparent thin-film electro-stimulative component as a modular expansion for the pneumatic mechanical stimulation platform described by J. Kreutzer et. al [13]. The final structure should create a modular electromechanical stimulation platform for stem cell research.

Hereby, it is of high importance that functional properties of the existing system are not compromised, but enhanced through a straightforward addition of an electro-stimulative module. Electrode materials applied for this task need to be highly stretchable and transparent to sustain the excellent mechanical and optical properties of the original mechanical stimulation system. Also, the material of choice needs to be easy to pattern, bond to PDMS, and be compatible with biofunctionalization procedures as well as relatively cheap and suitable for rapid prototyping.

Currently, there are no two dimensional biomimetic cultivation systems for electromechanical stimulation of stem cells reported in literature. The functional electromechanical cell stimulation system proposed in this thesis work is therefore a novel contribution to the field.

This thesis proposes two optional approaches, providing different functionalities due to their intrinsic properties, for the design of an electro-stimulative component: (1) Direct electrical stimulation (independent from mechanical stimulus) using transparent electrodes fabricated from conductive polymers and (2) indirect electrical stimulation coupled to the mechanical stimulus created by an embedded piezoelectric layer of cellulose nanocrystals (CNC). The envisioned electro-stimulative components should be integrated into the cell cultivation area by surface embedment into the polydimethylsulfoxide (PDMS) membrane. Fig. 2 illustrates the envisioned system design.

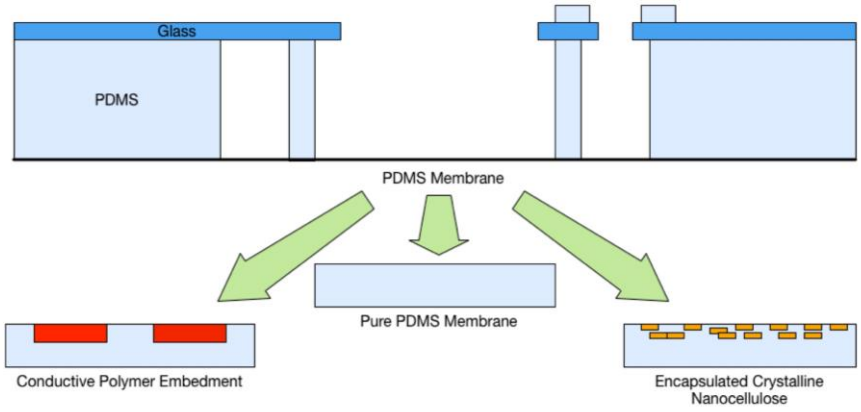

Figure 2. *Membrane integration strategies for conductive polymeric electrodes and CNC electro-stimulative layers.*

Direct controlled electrical stimulation of cells can be used separately or in combination with the mechanical stimulus. Poly(3,4-ethylendioxythiophene): polystyrene sulfonate (PEDOT: PSS) based conductive polymeric composites have been proposed as stretchable conductor for electrode fabrication [15]–[21] . PEDOT:PSS is a widely studied, solution processable conductive polymer commonly used for a variety of unconventional mechanically challenging applications in biomedical engineering [15]–[21].

In the second approach, the piezoelectric properties of CNC are utilized to create electrical charges coupled to the mechanical stimulus created. Cellulose nanocrystals, also denoted as nanowhiskers, are the smallest structural elements of cellulose fibrils. They have gained interest as a functional material throughout the recent years due to their intrinsic properties, functionality and biocompatibility. [22]–[25] However, CNC are more commonly utilized as reinforcement material for polymers, due to their mechanical stiffness [26]. The piezoelectric properties of CNC have been only gaining interest recently, as there are only very few reports about the piezoelectric properties of CNC available [26], [27]. To preserve the stretchability of the original mechanical stimulation system a novel fabrication strategy for an elastomeric nanocomposite based on CNC needs to be developed.

1.2 Thesis Structure

Following this introduction, Chapter 2 reviews the basic concepts of engineering in the stem cell niche, two dimensional (2D) biomimetic cell cultivation devices and their importance for the future of stem cell research, stretchable electronics, conductive polymeric materials as well as properties and capabilities of cellulose nanocrystals.

Chapter 3 covers the experimental set-up conducted during this thesis work. Obtained results and related discussions divided into sections according to the proposed structural approaches are covered in Chapter 4. The thesis is concluded in Chapter 5 with a general comparison of the system approaches.

2. THEORETICAL BACKGROUND

This chapter aims to present a throughout theoretical background related to topics covered in this thesis. It especially covers the role of the stem cell niche for the future of biomedical engineering. Developments in 2D biomimetic cultivation devices, especially systems realizing electromechanical stimuli, for recreating of the cellular microenvironment are covered in the following sections. The importance of stretchable electronics with a focus on graphene based polymeric conductors are described next. Finally, properties of cellulose nanocrystals as well as strategy for nanocomposite fabrication utilizing this material are introduced.

2.1 Stem Cell Niche

It has been widely proven that multipotent stem cells can be found in every tissue in the human body [28], [29]. These multipotent stem cells replenish the tissue with new functional cells to retain tissue integrity and assist during wound healing. The idea that specific regions in a functional tissue can retain their proliferation potential was the first description of a stem cell niche [28], [29].

The term “stem cell niche” is defined as an anatomical site containing a reservoir of multipotent stem cells for tissue replenishment and repair [28]. Hence, every tissue type in the human body forms its own specific stem cell niche. Cellular function is dependent on signaling cues from the cell-cell and cell-ECM connections formed throughout the tissue. Therefore, each tissue specific stem cell niche is a highly dynamic construct, as it carefully balances the formation of stem cells and progenitor cells during homeostasis. So not only the abundance of stem cells in a stem cell niche is important, but also the possibility to regulate stem cell behavior [28], [29].

In order to obtain and study realistic tissue like behavior of stem cells, it is of high importance to gain control over cellular expansion and differentiation. However, in standard *in vitro* cultivation technologies all cells are experience a similar ECM containing mainly biochemical cue variations and the representation of a physical framework containing ECM protein components, such as laminin, collagen and gelatin [30]–[32]. Mechanical strain or electrical signals, which cells in various tissues receive, have not been fully integrated in standard *in vitro* cultivation technologies so far [33]. Hence, cells cultivated with standard *in vitro* technologies due not express a realistic tissue like behavior and therefore fail as relevant physiological models.

2.1.1 Role of the Cellular Microenvironment

The extracellular microenvironment is formed by a complex network of macromolecules governing cell fate through their biochemical and physical properties. This network appears different depending on the type of specialized tissue. So cells and cellular progenition are directly responsive to the stimuli exerted by the ECM [32], [34], [35].

In addition to biochemical factors, physical stimuli exerted by the ECM include mechanical, optical and electrical cues. The interplay of all cues is the key to guiding stem cell fate and steering cellular behavior in regards to function, differentiation and tissue integration [32], [34], [35].

Mechanical cues from the ECM guide cellular shape, cell migration, morphogenesis and tissue orientation [30]. Especially cell types that exert mechanical work, such as myocytes and bone cells, need those mechanical cues during differentiation [34], [30].

Electrical cues are transmitted through a cell layer through gap junctions and stimulate the function of gated ion channels. Gap junctions, in nervous cells also called electrical synapses, are inter-cellular connections between cells in a tissue. They directly connect the cytoplasma of cells and allow molecules, ions and electrical impulses to be transmitted in a fast and controlled way. The presence of inter-cellular connections in a single-cell layer suggest a high level of cellular differentiation and tissue like behavior [28], [29]. Ion channels regulate the intra-cellular ion concentration and charge over cell membranes. So they are important for signal transduction between cells, especially cells in our nervous system and heart. [36]–[38]

The need for combined electrical and mechanical stimulus is not always directly apparent from cellular function. However, in many tissues those two systems need to be well-orchestrated to retain tissue functionality. For example, a well-orchestrated coupling of electrical signal conduction and mechanical contraction is necessary to create the blood pumping motion of the heart. Failure in the electromechanical transduction system can lead to arrhythmia and infarcts, which can lead to system failure and ultimately death [39], [40]. Also bone cells depend on a coupling of electrical and mechanical stimuli for differentiation and calcification. Ribeiro et. Al (2015) reported that crystal structures formed in bone cells during calcification act as piezoelectric materials [41]. Bone density varies depending on mechanical load distribution. Due to the piezoelectric properties of bone cells, mechanical stress applied to the bone results in an electrical impulse. This impulse regulates calcium channels and the gene response needed for calcification, ultimately resulting in a higher calcification rate of bone areas under mechanical load [41].

2.2 Two Dimensional Biomimetic Stimulation Systems

Stem cells cultivated with classic *in vitro* cell cultivation protocols [42]–[44] lack the complexity and degree of differentiation to function as reliable adult cell models. For the further development of stem cell therapy and drug testing platforms based on stem cell fate, novel cell cultivation technologies need to be found in order to grow highly differentiated cells and tissues from stem cells [45]. Engineering solutions for biomimetic cell cultivation platforms that recreate the complexity of cues expressed by the extra cellular matrix have been highly sought after during the last decade. Basic operation principles of 2D biomimetic cell cultivation devices for mechanical, electrical and elctromechanical stimulation are described below.

2.2.1 Mechanical Stimulation Platforms

Mechanical stimulation platforms rely on two distinct working methods: (1) mechanical properties (e.g. stiffness) of the substrate guide mechanical properties of the cell layer or (2) the substrate itself is stretched or compressed, stimulating cells grown on the substrate in the same magnitude, in a static or dynamic fashion [45], [31]. Both methods result in an intracellular strain, which guides cellular responses, including cellular alignment, structural orientation, gene expression and calcium handling [46]–[50]. A variety of systems utilizing different means of strain applications have been reported, including flow-induced shear forces, hydrostatic pressure, substrate topography and stiffness, cell indentation, and substrate stretching [46]–[48], [50], [49], [51], [52]. Many biomimetic stretching platforms utilize a stretchable elastomeric membrane connected to an actuator. For stretching actuation, mostly electrical actuators, such as a stepper motor, a DC motor or a voice coil actuator, are utilized for membrane deformation [53]–[56]. Pneumatic actuation methods, on the other hand, have only been reported very recently [9], [13], [57]. However, the engineered stretching platforms are in general quite bulky, as the most common actuation methods relies on a stepper motor to strain an elastic membrane.

2.2.2 Electrical Stimulation Platforms

Electrical stimulation systems rely on a rather simple design. Most commonly they consist of two electrodes immersed in the culture container. An electrical field is formed between the electrodes mediated by the ion concentrations in the culture medium [58]. This electrical field causes electrical stimulation of cells, commonly applied to neuronal cells, muscle cells and cardiomyocytes [37], [38], [59]–[64]. Electrical stimulus accounts for the duration of action potentials and reactive calcium channels [58], which guides signal transduction within a tissue. However, electrical stimulation also strengthens tissue connectivity and synchrony [58].

2.2.3 Electromechanical Stimulation Platforms

Two dimensional electromechanical stimulation systems have not yet been described in literature as there are concerns regarding the coupling dynamics of both forces. However, there are three dimensional cultivation systems developed for electromechanical stimulation of cardiomyocytes available [58], [58], [65], [66]. Hydrogels are used as cultivation scaffolds in those systems. Mechanical stimulus is then applied either by direct deformation of the hydrogel or shear stress caused by a fluid flow through the hydrogel matrix. Coupled electrical stimulus can be applied through an electric field formed between two electrodes [40], [66] or piezoelectric materials embedded into the hydrogel matrix [67].

2.3 Stretchable Electronics

Technological innovation in electronics throughout the last century fully exploited the capabilities of classic electrical systems, which are rigid structures fabricated on glass and silicon substrates. Modern electronics become progressively integrated in our everyday life, causing a strong motion to rethink human technology interactions. At the current point in time, we are interacting with technology and electronics mostly via flat, rigid surface. However, objects surrounding us in everyday life are usually consisting of curved surfaces, perfected in their design by practical use. To allow a more humane interaction with modern technology electronic systems need to be integrated in such curved surfaces. Next-generation electronics will be therefore fabricated on polymeric foils creating flexible, bendable and even stretchable electronic systems. First developments in this direction have been done by introducing wearable technologies, such as curved screen systems, intelligent textiles and wristlet systems.

The importance of this system transition becomes especially apparent in biomedical systems. First steps in this direction haven been done with the development of artificial skin, including a wide range of intelligent sensing and control systems [68], [69]. For the creation of skin-like structures, sensors and electronics need to be extremely flexible to accommodate the twisting, bending and stretching motions of natural human skin. So electronics need to express a rubber-like, stretchable behavior in order to fulfill the requirements of next-generation electronics.

A classic approach for the fabrication of stretchable electronics is the creation of pop-up structures, meaning three dimensional electronic interconnects made from classical stiff conduction materials, such as copper or gold, on a stretchable substrate. The interconnects are fabricated in a way that they form a wavy ribbon structures elevated from the surface. When the substrate is stretched, these wavy ribbons elongate and flatten to accommodate the in-plane surface strain [70]. As such systems are based on well-known electric conductors (metals), the fabricated electronic structures are easy to characterize and handle.

However, they can only withstand a certain amount of intrinsic strain and limit the transparency of electronic devices, which is especially of interest in single-cell sensing applications [70].

Another approach for the creation of stretchable electronics is the application of conductive polymers. Conductive polymers are organic materials featuring conjugated structures capable of electronic conduction. Their conduction properties highly depend on their synthesis conditions, such as polymerization temperature and doping. The fabrication of conducting elastomers, by adding conductive fillers to a rubbery polymer, is also a possible strategy to fabricate stretchable electronics. Elastomers, such as Polydimethylsulfoxide (PDMS), can accommodate relatively high strains. Conductive fillers incorporated into elastomeric polymers range from carbon particles, carbon nanotubes (CNT), graphene flakes, graphene sheets and cellulose nanocrystals [70]. Another approach is the formation of conductive stretchable networks on top of a PDMS substrate made from CNT [30-32], graphene or nanowires [28-29]. Such structures have a high conductivity, but only medium transparency, which makes them challenging to use in single-cell analysis as well.

PDMS is the most widely utilized elastomer in microfabrication. It is commonly used in prototyping of microsystems, including microfluidic chips and biomedical microelectromechanical systems (bioMEMS). It is also the base material for soft lithography applied in transfer techniques such as micro contact printing and surface patterning of soft actuators [70]. PDMS has a hydrophobic nature [76], with a water contact angle of 116 ± 1° [70] and therefore low wettability. This low polarity also makes the material chemically inert for aqueous solutions and a challenging material to use as a base for fabricating composites [77]–[79]. However, PDMS surfaces can be easily turned hydrophilic by exposure to ultra violet (UV) light, ozone, corona or oxygen plasma discharges [70]. Elastic properties of PDMS strongly depend on its synthesis conditions, especially mixing ratio between polymeric base and cross linker. The most commonly applied mass fraction (w/w) ratio 10:1 results in an elastomeric modulus of 1.1 MPa [3]. However, this elastic modulus also depends on the elastomer thickness. So have PDMS structures with a thickness below 1 mm higher elastomeric moduli than structures ranging above 1 mm in thickness [70].

2.3.1 Conductive Polymers

Stretchable polymeric conductors have gained interest in all kind of applications that are out of scope with classic silicon technologies, due to the rigidity of silicon processed materials. Conductive polymers are biomaterials with inherent conductivity and relative softness. During fabrication, their physical properties can easily be tailored by varying the process parameters, making them easily adaptable for a wide range of specific applications.

Conductive polymers show, depending on their optimal conformation, high electrical conductivity, low ionization potential, high electronic affinities and superior optical properties (transparency) [80]–[82]

The intrinsic conductivity of conductive polymers, is caused by their matrix structure, which has a high degree of overlapping in molecular orbitals. These permit the formation of a dislocated molecular wave function throughout the polymer matrix. Electrical properties depend on the percentage of doped ions in the molecular matrix, which is usually achieved by chemical or electrochemical oxidation of a monomer [80]. Conductive polymers applied include polyparaphenylene, polyphenylene sulphide, polypyrroles and poly(3,4-methylenedioxythiophene) [80].

In addition to their physical properties, conductive polymeric materials are of high interest for biomedical engineering due to their capability to easily bond biomolecules [80]–[85]. They were even found to enhance the sensitivity, stability and speed of biomolecular reactions [86]–[88]. Functionalization techniques for conductive polymeric materials range from non-covalent bonding procedures to covalent attachment protocols utilizing 1-Ethyl-3-(3-dimethylaminopropyl)carbodiimide and N-hydroxysuccinimide coupling chemistry [86]–[88].

PEDOT:PSS is a widely studied, solution processable conductive polymer commonly used for a variety of unconventional mechanically challenging applications in biomedical engineering, such as fabrication of electronic skin [19-20], bioMEMS fabrication for electrical stimulation of neuronal cells [17] and thin film sensor fabrication for biosensing [22-25]. Its chemical and mechanical properties [26-27] make it a beneficial conductive polymer. Even though native PEDOT:PSS has only a limited stretchability [21], the conductivity and stretchability [21], [26-27] of PEDOT:PSS ink can be easily enhanced by incorporation of graphene to form a nanocomposite structure of excellent electrical and physical properties.

2.3.2 Graphene Nanocomposites

Graphene is considered to be an excellent nanofiller for conductive composite materials due to its high thermal conductivity, excellent mechanical properties, high surface area, high aspect ratio, high tensile strength, high electronic transfer properties and transparency [91].

Graphene is a two-dimensional layer of carbon atoms packed densely in a honeycomb lattice. The sheet consists of sp^2-bonded carbon atoms. Due to its geometrical structure, graphene is regarded as thinnest functional material and has exceptional physical and chemical properties [70]. Furthermore, it is produced from relatively low cost graphite without harmful byproducts, which makes it interesting for commercial applications. [91] For nanocomposite fabrication, it is preferred due to its conductive properties at

low filler concentrations, which lie significantly above classical nanofillers such as carbon particles and cellulose nanofibers. [70] Only CNTs show comparable electrical conductivity. However, due to the high production cost of CNTs graphene can still be considered a superior material.

The electrical conductivity of graphene reinforced nanocomposites is enhanced, because graphene enables the formation of conduction paths between its sheets or flakes. This has been observed in bare graphene [28-29] and CNT films [71]–[73] and it can be expected that similar effects take place within the polymer matrix. However, the effectivity of this process strongly depends on interfacial adhesion between the polymer matrix and graphene sheets and therefore the integration capabilities of graphene, as they dictate the final properties of the prepared nanocomposite. Pristine graphene sheets tend to agglomerate in a polymeric matrix, which makes them not compatible with the fabrication of homogenous polymer blends. To ensure a homogenous and easy dispersion in the polymer matrix, graphene sheets are functionalized with, for example, small polymer chains or molecules [91]. Applications of graphene/PEDOT:PSS polymeric blends as electrode material for piezoelectric thin-film sensors [26-28] and photonics [89] were recently demonstrated.

2.4 Cellulose Nanocrystals

Plant derived fibers haven been used by humanity for thousands of years for a variety of applications. Even nowadays, cellulose remains the most abundant renewable polymer resource available. The chemical structure of cellulose is described for around 150 years [95] leading to its aimed modification and application. However, the fact that after chemical reduction of cellulose, its smallest chemical components are rod-shaped crystalline structures, is only known for a couple of years [95]. CNC, also frequently denoted as nanowhiskers, have not only excellent physical and chemical properties, but are also a sustainable, renewable material. Hence, the material gained interest recently for polymeric composite reinforcement [96]–[102] as well as other applications.

2.4.1 Structure and Fabrication of Nanocellulose

Cellulose can be found in nature in different degrees of complexity. In higher degrees, it is available in the cellular wall of all plants and some marine animals (tunicates) [95]. In less complexity, it is produced by algae, fungi, bacteria and invertebrates [95]. In general, cellulose is a fibrous, stiff, water in-soluble material, which varies in structure depended on its source.

Cellulose is a natural homopolymer of high molecular weight built from β-1,4-linked anhydro-D-glucosepyranose units with a spatial offset of 180° in regards to their neighbors. Hence, cellulose fibers assume a stable helical configuration. Due to a variety in

terminal ends, every cellulose chain has a reducing and oxidizing (hydroxyl (OH) group) functional terminal group. All β-D-glucopyranose units adopt a $^4C_1$ chair conformation, which are chained and stabilized by intramolecular hydrogen bonds through glycosidic linkage. During biosynthesis, cellulose chains are entwined to form microfibrils of 2 - 20 nm length, which are undergoing crystallization stabilized by strong Vander-Waals forces as well as inter- and intra-molecular hydrogen bonds [95]. Microfibrils in full crystallinity are forming the smallest chemical component of cellulose fibers – cellulose nanocrystals. This chemical structure, especially the surface presentation of strongly polarized OH-groups, makes CNC highly reactive materials suitable for a variety of surface modifications, such as silanization [103]–[105], esterification [95] and biofunctionalization [25], [106]–[109]. Subsequently, cellulose nanocrystals form longer cellulose nanofibrils (CNF) formed by chaining of CNC behind each other through weaker chemical bonding (amorphous regions). In plants, multiple CNF are then intertwined to form cellulose fibrils and sub-sequent cellulose fibers.

For engineering applications, CNC can be obtained by two approaches: bottom-up through biosynthesis of nanofibrils by bacteria or fungi, or top-down through mechanical and chemical degeneration of plant material. In the bottom-up approach, CNC and CNF are formed by biosynthesis in a controlled environment. [95] However, this method is time consuming and costly, as the bacteria or fungi need to be cultivated for several weeks to achieve any amount (some milligram to gram) of material. In comparison, the top-down approach is more cost efficient as large yields (several kilogram) can be processed at once. [95] This top-down approach is schematically described in Fig. 3 for wood fibers.

For that, cellulose fibers found in the cell walls of wood are mechanically disintegrated to cellulose fibrils and CNF. The amorphous regions in cellulose nanofibrils are then chemically dissolved using acid hydrolysis. For that, CNF are cooked in high concentrated acid, such as sulfuric or hydrochloric acid, at elevated temperatures. In the process, amorphous regions are hydrolyzed, while crystalline regions, which have a higher acid resistance, remain intact [95]. Pretreatment and acid hydrolysis conditions depend on the type of fiber utilized [95].

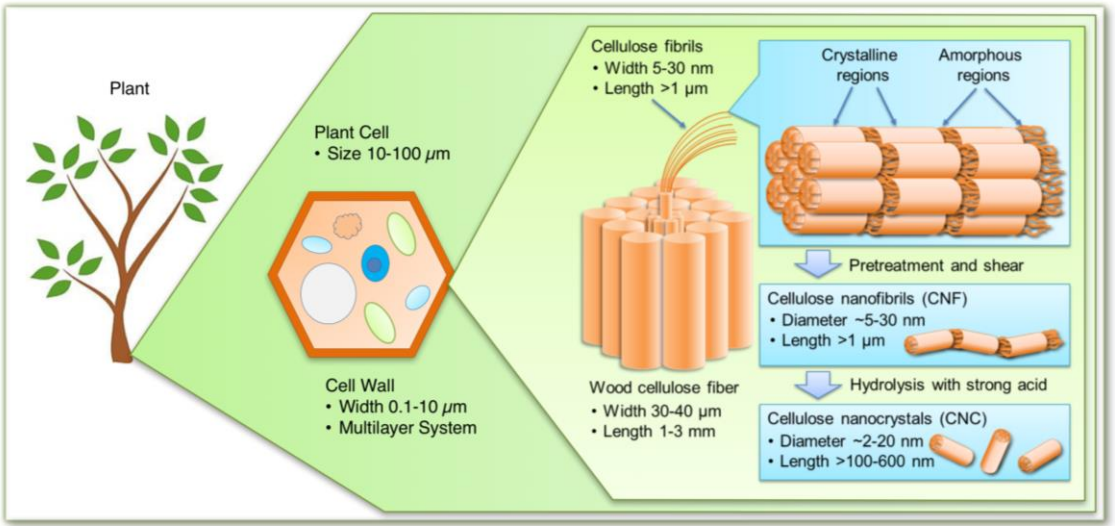

Figure 3. *Extraction of wood-based cellulose nanocrystals. Through mechanical milling wood cellulose fibrils are extracted from the cell wall of a plant cell. Cellulose fibrils are actually fiber bundles consisting of crystalline and amorphous structural regions. Fibril bundles are broken into separate cellulose nanofibrils through shear strain. Through chemical hydrolysis amorphous cellulose regions are dissolved and cellulose nanocrystals retained. (Adapted from* [110]*)*

2.4.2 Properties of Nanocellulose

Mechanical and therefore functional properties of CNC are strongly determined by their unique structure and chemical properties described earlier. As previously mentioned, CNC are rod-shaped, monocrystalline structures. Depending on their source and preparation method, they differ in dimension: Bacterial nanocellulose crystals have a length of 100-1000 nm and width of 10 – 50 nm [111], while CNC originating from wood fibers are 100 – 600 nm in length and 2 – 20 nm width [24].

CNC are stiff materials, due to their high surface area to volume ratio caused by their crystal conformation, high density of covalent bonds per area and strong inter- and intra- molecular forces. Various theoretical approaches to estimate the axial modulus of cellulose have been done [25]. Strain modulus values range from 58 – 180 GPa [25] for single cellulose crystals to 300 GPa [112] when considering intra-molecular forces.

The chemical bond structures of CNC relies on a hydrogen saturation in the crystal bonds [95]. This renders CNC in-soluble in water. However, due to the abundance of OH-groups CNC crystals are hydrophilic, causing them to self-align in an electrostatic stable conformation (helical structure) in aqueous solutions given enough time [95]. Their functional groups also make them highly interesting materials for surface functionalization procedures [25], [95], [103]–[109].

Piezoelectricity of Nanocellulose

Piezoelectricity is defined by the occurrence of dipole moments and change of polarization density in crystalline materials in response to mechanical stress. Hence, piezoelectricity is a cross-coupling effect between dielectric variables (electric field and electric displacement) with elastic variables (stress and strain) [113]. Due to the crystal structure of native CNC, it can be expected that the material has piezoelectric properties [26].

Piezoelectric properties originating from crystalline regions of wood fibres were already reported in the 1950´s [114]. However, first experimental validations of those properties in CNF [115] and CNC [26], [27] films were only published very recently.

Piezoelectricity of a material depends strongly on the symmetry of its crystal lattice, as the piezoelectric sensitivity is expressed as an overall material value. This effect is expressed using the piezoelectric coefficient d_{mn}, which is directly related to the electrical field produced under mechanical stress. The piezoelectric coefficient is conventionally expressed as a 3 x 6 matrix, with m = 1 - 3 referring to the electrical axis and n = 1 – 6 referring to the mechanical axis [113]. Symmetry in a crystal lattice however reduces the number of independent piezoelectric coefficients leaving only reactive axis as finite values. The theoretical piezoelectric coefficient for wood [114] is shown in Eq. 1, which takes into account monoclinic C2 symmetry and cancellation effects of the crystal lattice. It becomes apparent that only the shear piezoelectric constant ($-d_{14} = d_{25}$) are finite, while all other matrix components go towards zero.

$$d_{mn} = \begin{pmatrix} 0 & 0 & 0 & d_{14} & 0 & 0 \\ 0 & 0 & 0 & 0 & d_{25} & 0 \\ 0 & 0 & 0 & 0 & 0 & 0 \end{pmatrix} \quad (1)$$

Therefore, it is important to consider crystal orientation in a fabricated CNC material, as only shear strains caused, for example, by material bending result in a piezoelectric response of CNC. For the fabrication of functional defined nanocomposites, CNC orientation is of high importance. Crystalline orientation, however, varies between materials. So is the piezoelectric constant in wood insignificantly small, as the crystalline regions are randomly distributed and only available in small amounts throughout the heterogeneous wood matrix [114]. CNF materials show higher piezoelectric constants approximately 5 -7 pC/N [115]. The piezoelectric constant of single CNC however was reported to be approximately 35 – 60 pC/N [26], which compares to the piezoelectric coefficient of polyvinylidene fluoride (PVDF) (d_{33} = -33 pC/N [116]), a heterogeneous piezoelectric polymer used for example in in energy harvesting applications [117].

2.4.3 Nanocellulose Composites

Due to its nanoscale dimensions, high surface area, mechanical stiffness, functionality, in-solubility in water, biocompatibility, degeneration and renewability, nanocellulose has gained interest as reinforcement material for the production of high performance biocomposites. Nanocellulose has been successfully integrated as filler material into a wide range of polymeric matrixes, including polysiloxanes [105], polysulfonates [95], polyurethane [118], polyethylene [100], and biopolymers, including starch and protein based materials [119], [98] and chitosan [97]. It has been also integrated in biopolymer-like materials often used in tissue engineering, such as poly(hydroxyoctanoate) [120] and poly lactate [121], [122].

Two general fabrication strategies for nanocellulose composite types can be identified from literature: (1) total reinforcement through mixing nanocellulose with a polymeric matrix [23], [99] and (2) surface adhesion of CNC on an anchoring layer mediated through electrostatic adsorption and wettability capabilities of the material [123], [124]. Total polymeric reinforcement thrives to create composites, which contain CNCs homogenously distributed throughout the matrix. This can be achieved either by solvent evaporation [95] or sol-gel casting [96] techniques. As CNCs are not directly miscible with most resin and polymeric matrixes [95], [99], due to their polarity, dry CNC networks in the form of thin-films or aerogels are fabricated by solvent evaporation [125]. The dry crystals are then either homogenously dispersed or incorporated by direct casting in the polymeric matrix. The second nanocellulose composite fabrication strategy relies on the formation of thin CNC layers on a prepared substrate [103], [123], [124]. Substrates are conventionally polymeric, but also resin, glass or biopolymers have been used. Prior to CNC application, the typically hydrophobic substrate is physically or chemically treated to form an anchoring layer that enhances wettability and electrostatic properties of the substrate [107], [98], [122], [123], [126]. Aqueous CNC suspension is then layered onto the substrate most commonly by spin coating, spin casting or droplet coating [123] and dried. Such surface adsorbed CNC layers are usually very brittle due to the intrinsic properties of CNC. Depending on the fabrication method and desired structural properties, CNC concentrations ranging from 30 % w/w [25] to 0.05 % w/w [123] have been used. In general, a higher percentage of CNC solids are needed for the reinforcement of thick composites than for the fabrication of thin films.

Both described fabrication strategies suffer heavily from adhesion problems when CNC without surface treatment, either of the crystal or the substrate, is applied [126]. Due to the strongly polarized OH groups in CNC, the material is hydrophilic. However, most polymeric materials are hydrophobic and therefore immiscible with polar solutions. This leads to an ineffective interfacial adhesion between the polymeric matrix and nanocellulose crystals, leading ultimately in a different stress loading and failure of the material. Several strategies to improve the compatibility between polar CNC and non-polar matrixes have been proposed [126]. Most commonly, chemical surface modifica-

tions [95] of cellulose nanocrystals with organic solvents are applied. In those, the OH-groups on the crystal surface are chemically modified by, for example, silanization [103]–[105] or esterification [95], which improves surface compatibility. Also physical modification strategies have been proposed, including surface oxidization with cold plasma [123] or corona treatments [126]. Such treatments enhance the wettability of not only CNC, but also most polymeric surfaces and can therefore be applied on both for adhesion promotion. Such techniques are most common in nanocomposites relying on CNC thin-films.

3. EXPERIMENTAL

This chapter gives an overview on the experimental procedures conducted during the thesis work. It is divided into three main parts: (1) fabrication, operation and characterization of the equiaxial stretching device used as basis for this thesis, (2) material integration and functional characterization of stretchable electrodes fabricated by a conductive polymeric ink and (3) fabrication and characterization of a novel, piezoelectric PDMS-CNC composite membrane.

3.1 Equiaxial Stretching Device

The experimental work in this thesis thrives to integrate an electrical stimulative module into the equiaxial stretching device developed earlier by J. Kreutzer et. al [13]. Hence, all new system functionalities should be compatible with the original system design and therefore their implementation strongly depends on its underlying characteristics. The following sections shortly summarize fabrication, operation principle and characterization of the equiaxial stretching device.

3.1.1 Device Fabrication

The basic equiaxial stretching device (denoted stretcher in the following sections) developed by Kreutzer et. al [13] is a stand-alone system, in which a thin PDMS membrane is stretched via an applied partial vacuum pressure. The system can be divided into two main functional component groups: (1) the stretcher base consisting of two concentric PDMS shells bonded to a glass cover plate, which form the cell stretching and vacuum chamber, as well as (2) a thin, transparent, stretchable PDMS membrane (d = 120 μm).

Fig. 4 shows dimensions and working principle of the assembled stretcher. The inner concentric shell defines an active cell stimulation area of 113 mm^2 (D = 12 mm) and has a wall thickness of 1.5 mm. This allows the inner shell to buckle outwards when the partial vacuum is applied in the vacuum chamber. The vacuum chamber has a thickness of 3 mm in order to allow sufficient space for the buckled membrane. The outer PDMS shell has a thickness of 13 mm and stabilizes the complete system. The inner and outer PDMS shells have a height of 7 mm and are irreversibly bonded to a 1 mm thick glass cover plate. This cover plate has an opening above the cell cultivation area (D = 10 mm). Otherwise it covers the complete system, only allowing a 1 mm wide drilling in the vacuum chamber to apply a partial vacuum to the stretcher.

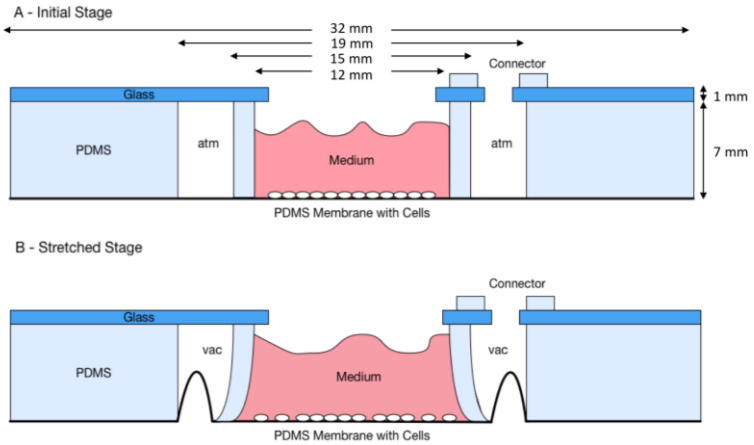

Figure 4. *Schematic working principle and dimensions of the pneumatic equiaxial stretching device. (Adapted from* [13]*)*

In total, the circular system design resembles closely traditional cell culture plates (petri dish, multi-well plates) used in *in vitro* cell cultivation [44], [127].

PDMS (Sylgard 184, Dow Corning, USA) was utilized for prototyping the shell structures and membrane. Hereby, a standard preparation protocol was applied. The silicone elastomer pre-polymer (base) was mixed with the cross-linker (curing agent) vigorously in a 10:1 mass ratio. Trapped air, resulting from the previous step, was removed from the mixture by vacuum application for approximately 20 min. Then the mixture was poured into a closeable disk mold (D = 32 mm) for shell fabrication and spin-coated for membrane fabrication. After that, the PDMS mixture was cured for 10h at 60°C in an oven (Binder GmbH, Germany).

The concentric shells were fabricated utilizing a closed disk mold with laser cut edges. Shells were punched from the fabricated PDMS disk using custom made punching tools to fabricate the structure described earlier. Cavities for the cell cultivation area and vacuum connector were manually drilled in a circular glass cover plate (d = 1 mm, Aki-lasi Oy, Finland) with a diameter corresponding to the system (D = 32 mm). Then, the shells were irreversibly bonded to the prepared cover plate using oxygen plasma (Diener Electronic GmbH, Germany) at 0.3 mbar and 30 W for 15 s. To ensure tight connections with the vacuum tubing (D = 3 mm), a PDMS plug was bonded above the vacuum connector cavity utilizing the same process. This concluded the stretcher base assembly.

For reliable and repeatable fabrication of the stretchable PDMS membrane, PDMS was spin-coated (Modular Spin Processor WS-400A–6NPP, Laurell Technologies Corp., USA) on a sturdy polystyrene (PS) plate in a three-step protocol: (1) 20 s at 200 rounds per minute (rpm), (2) 30 s at 700 rpm and (3) 10 s at 100 rpm. Tailoring of the membrane structure for integration of an electro-stimulative component was done during this fabrication step throughout the following experimental set-up.

After curing, the assembled stretcher base was irreversibly bonded to the membrane using oxygen plasma at 0.3 mbar and 30 W for 20 s. Finally, the assembled system was carefully removed from the PS plate to be used in stretching experiments.

3.1.2 Stretching Procedure

Controlled partial vacuum pressure is applied to the stretcher using an in-house built pressure regulation set-up described earlier in [13]. Fig. 5 illustrates the utilized vacuum operation system. The pressure regulator has a performance range of maximal 392 mbar partial vacuum pressure (2 bar over pressure) with an accuracy of 0.1 %, repeatability of 0.1 % and rise time of 20 ms.

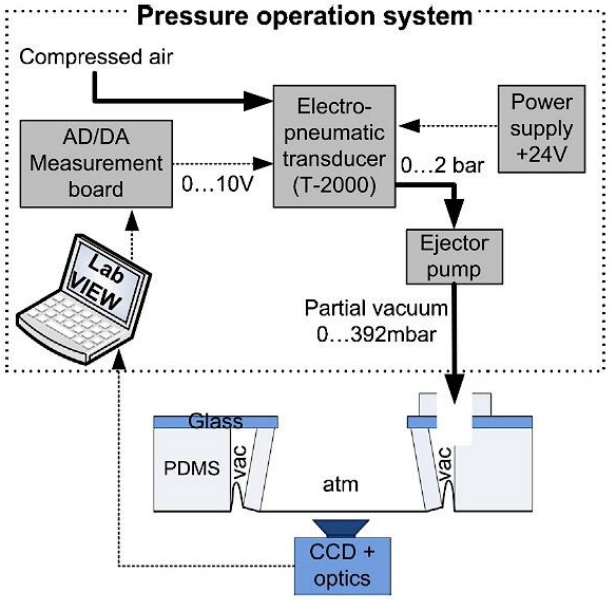

Figure 5. *Vacuum operation system in connection with the equiaxial stretching system. (Taken from* [13]*)*

Under these conditions, the reported maximal static in-plane strain ε_P of the system is 9.5 % ± 0.3 % [13] at 392 mbar. However, for simplification purposes and to accord for probable strain variations due to varying system fabrication tolerances, a maximal static in-plane strain of ε_P = 10 % is assumed during the following experiments. As reported in [13], strain values increase linearly to the maximal in-plane strain throughout the pressure range.

For testing, the systems were stretched in a stepwise procedure between 0 – 392 mbar in 50 mbar increments. Between each pressure point, a static strain was maintained for 2 – 5 min.

3.1.3 In-Plane Strain Analysis

Characterizing the stretchers in-plane strain directly at the membrane is of high importance, as it allows evaluation of the mechanical stimulation capabilities of the system. Cells cultivated on the system membrane are expected to experience the same type of deformation as the membrane itself. Hence, any structural changes applied to the membranes conducted in the following experiments might influence mechanical stimulation performance of the system in a major way.

For membrane characterization, landmarks using fluorescent polymeric microspheres were added to the stretcher. Dragon Green fluorescent microspheres with c = 0.01 % solids (D = 4.18 µm ± 0.397 µm, Dragon Green (Ex.: 480, Em.: 520), Bangs Laboratories, USA) in aqueous solution were applied to the PDMS membrane (system bottom) and strongly adhered via physisorption. After drying, the system was stretched in a step-wise manner and optical microscopy images were taken using the fluorescence set-up of the AxioObserver.Z1 (see section 3.6) and a 100x magnification.

The in-plane strain was calculated using manual landmark recognition particle trajectory analysis in Fiji [128], [129]. The strain was calculated for a population of n = 3 samples and 10 landmarks per sample ranging in location from the middle to the outer edge of the cell cultivation chamber following the same analysis method described by Kreutzer et. al [13] to ensure comparable results. Centroid position coordinates (x, y) of the landmarks were recorded and the trajectory distance calculated for each applied pressure. By comparing the trajectory distances for each pressure point and landmark, the total in-plane strain ε_P of the structure is calculated. In Eq. (2) the trajectory distance (L_T) is illustratively calculated utilizing the x, y coordinates of the landmarks l_1 and l_2.

$$L_{T,12} = \sqrt{(x_{l1} - x_{l2})^2 + (y_{l1} - y_{l2})^2} \tag{2}$$

The resulting in-plane strain ε_P between the two landmarks l_1 and l_2 is then calculated by comparing the trajectory distances between them at a defined pressure to their positions at zero pressure, as shown in Eq. (3). The total in-plane strain was then calculated by comparing all strain components as illustrated in Eq. (4). The average in-plane strain presented in this thesis was then averaged over all three samples by comparing ten landmarks per sample.

$$\varepsilon_{P,l12} = \frac{\Delta L_T}{L_T} = \frac{L_{T,12} - L_{T,012}}{L_{T,012}} \tag{3}$$

$$\varepsilon_P = \frac{\varepsilon_{P,l12} + \varepsilon_{P,l23} + \varepsilon_{P,l13}}{3} \tag{4}$$

3.2 Fabrication of Stretchable Electrodes

This section focuses on the fabrication and functionality characterization of stretchable electrodes fabricated from a solution processable, conductive, polymeric ink on the PDMS membrane od the stretcher. The general content of this chapter has been object of a conference paper originating from this thesis work [130]. In order to present this thesis as a uniform approach, the main content of the publication is presented supported by some non-published data.

3.2.1 Conductive Polymeric Ink

For electrode fabrication, the commercial available conductive graphene ink MSDS P3014 (Phene^{TM} Plus Series, Innophene Co., Thailand) (denoted as Innophene in the following sections) was utilized. The ink is composed of homogenously distributed graphene flakes (< 1 %) mixed into a PEDOT:PSS polymer matrix (1-5 %) dissolved in organic solvents (66 – 95 %) [131]. Originally formulated for inkjet printing, the ink appears as a dark blue liquid. However, after crystallization (cross-linking), stable flexible electrode layers are formed that do not dissolve in aqueous solvents. The ink was applied as purchased without additives.

3.2.2 Conductive Polymer Electrode Fabrication

The hydrophobic nature of PDMS [76] renders the fabrication of well-adhered films from solution processable materials on PDMS as very challenging [132]–[134]. Therefore, harsh chemical surface treatments [133], [135] are frequently applied to render PDMS compatible for the fabrication of stretchable electronics. However, there is a risk that such treatments promote cell death, or at least growth inhibition, at a single-cell level. For the purpose of simplicity, and to ensure best possible conditions for single-cell survival, this thesis aims to incorporate and study stretchable electrodes from conductive polymeric material on a thin PDMS membrane without excessive surface pretreatment. The only adhesion promoting step was to render the PDMS surface hydrophilic by applying oxygen plasma (pressure: 0.3 mbar, power: 30 W, duration: 120 s).

This study distinguished between two different electrode designs and related ink integration strategies: (1) fabrication of large electrodes that cover the complete active surface of the stretcher (D = 12 mm), fabricated by large area thin-film processing methods, such as spray coating and spin coating, and (2) small patterned electrodes covering the active area only partially, fabricated by using a soft lithography approach. Finally, four different deposition strategies, two per type, are compared regarding their integration capability and functionality.

For large area electrode deposition, spin coating and spray coating of Innophene on a cured, oxygen plasma treated PDMS membrane was compared. These deposition tech-

niques were conducted prior to assembly of the stretching device to the stabilized PDMS membrane in order to achieve evenly distributed electrodes.

For spin coating, the hydrophilic PDMS membrane was placed into a spin coater (Modular Spin Processor WS-400A–6NPP, Laurell Technologies Corp., USA). Then 250 µl of ink was deposited in the middle of the membrane and distributed in a three-step spin coating protocol: (1) 10 s at 200 rpm, (2) 30 s at 500 rpm and (3) 10 s at 100 rpm. Optically similar layers were achieved through spray coating of Innophene at a pressure of 3 bar on a 60°C heated (standard hotplate) hydrophilic PDMS membrane. After deposition, the inks were allowed to crystallize at 60°C for 20 min in an oven. After partial crystallization (5 min in oven), layer built-up of ink material was possible by repeating the deposition procedure for both cases.

For patterning areas with conductive ink, soft lithography techniques [136] in the form of channel casting were applied. For soft lithography applications, a specifically patterned PDMS structure is fabricated from a photoresist mold, which was directly filled with electrode ink. Fig. 6 illustrates the fabrication procedure of a soft lithographic PDMS master starting from photolithographic mold fabrication. Photolithographic molds were fabricated in the new clean room facilities (class 1000) of Tampere University of Technology (Finland) under controlled atmospheric conditions. For hard mold fabrication, a silicon wafer was cleaned by oxygen plasma (30 s at 95 W, 320 Mk II RIE, Advanced Vacuum Vision AB, Sweden) and then the negative photoresist Su-8 was spin coated (Modular Spin Processor WS-650Hzb-23NPPB, Laurell Technologies Corp., USA). After a pre-baking step on a standard hot plate, which settled the SU-8, the photoresist was exposed to UV radiation (350 W UV Lamp, OAI 500 mask aligner, USA) through a patterned chromium photo mask. Exposed areas cross-link due to the UV radiation through the following post-bake procedure. After dissolving non cross-linked photoresist with a photoresist specific developer and a final hard bake at 120 °C for 45 min in an oven, the specifically patterned mold was ready to use. To ensure that the SU-8 mold fits the theoretical dimensions, microfeatures were measured with a contact profilometer (Dektak XT stylus profilometer, Bruker GmbH., Germany) with its settings set to the theoretical mold height. Also a quality control using an upright optical microscope (Axio Imager.A1m, Carl Zeiss GmbH., Germany) at 200x and 500x magnification was conducted. During PDMS master preparation, PDMS which was prepared with the same general procedure described in Section 3.1.1, was molded on the structure. After curing, the PDMS can be removed from the mold and has a negative of the mold structure embedded in its surface.

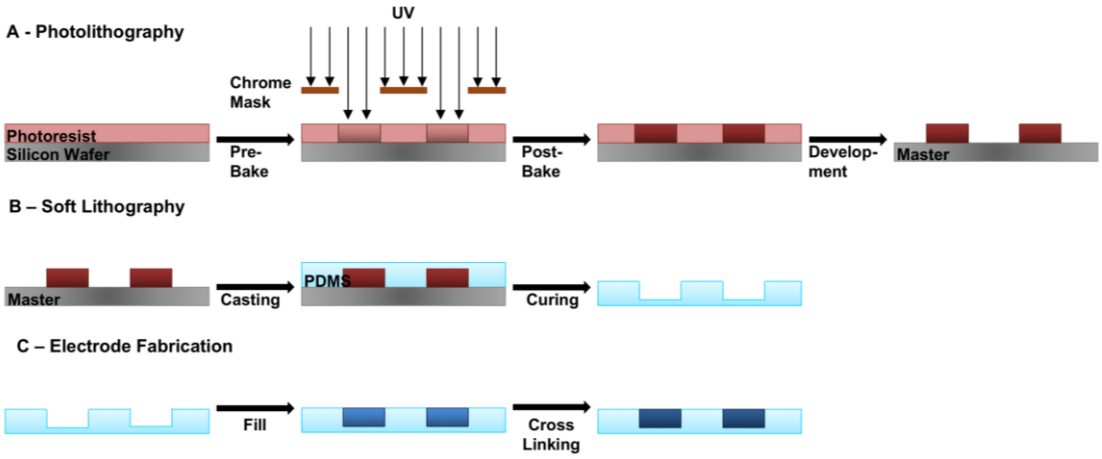

Figure 6. *Working procedure for channel casted electrode fabrication. A specifically micropatterned master mold was fabricated using a photolithographic process (A). This master represents a positive version of the desired structure. The desired channel structure was then transferred to PDMS through a soft lithographic process (B), in which PDMS was casted onto the master mold resulting into a negative copy of the mold. Finally, the negative PDMS channel structure was filled with solution processable conductive polymer for electrode fabrication (C).*

The photoresist mold for channel casting was specifically designed to fit the cell cultivation area of a stretcher. As illustrated in Fig. 7, the mold consist of four electrode structures, each containing two wire connection pads connected by a straight channel (l = 1 mm, w = 50 µm) forming an overall dumbbell structure. This design is aimed to aid the functionality testing of Innophene during stretching. The photoresist mold was fabricated under the following conditions: photoresist SU-8 3040 (MicroChem Corp., USA), spin coating: (1) 15 s at 500 rpm, (2) 40 s at 1400 rpm and (3) 10 s at 100 rpm 5 min at 70 °C and 45 min at 95 °C pre-bake, 32 s UV exposure, 5 min at 70 °C and 10 min at 95 °C post-bake and 10 min structure development. In the soft lithographic step, PDMS membranes were directly fabricated on the SU-8 mold. After curing, the membranes were cut to the correct stretcher size (D = 32 mm), peeled-off from the mold, flipped in order to have the structure facing upwards and placed on a stabilizing PS plate. The membranes were used during stretching system assembly, resulting in a system with a patterned membrane in the cell cultivation area. Prior to channel casting, the assembled stretching system was treated with oxygen plasma for the duration of 120 s at 30 W to ensure hydrophilicity of the PDMS membrane. Following activation, the systems were placed on a 60°C hotplate for 5 min to pre-heat. For channel casting, 20 µl of Innophene was carefully pipetted on the inner connector pad of each dumbbell electrode. Capillary forces then filled the channel and the remaining connector pad with ink. The channel casted structures were left on the hotplate for crystallization for 20 min.

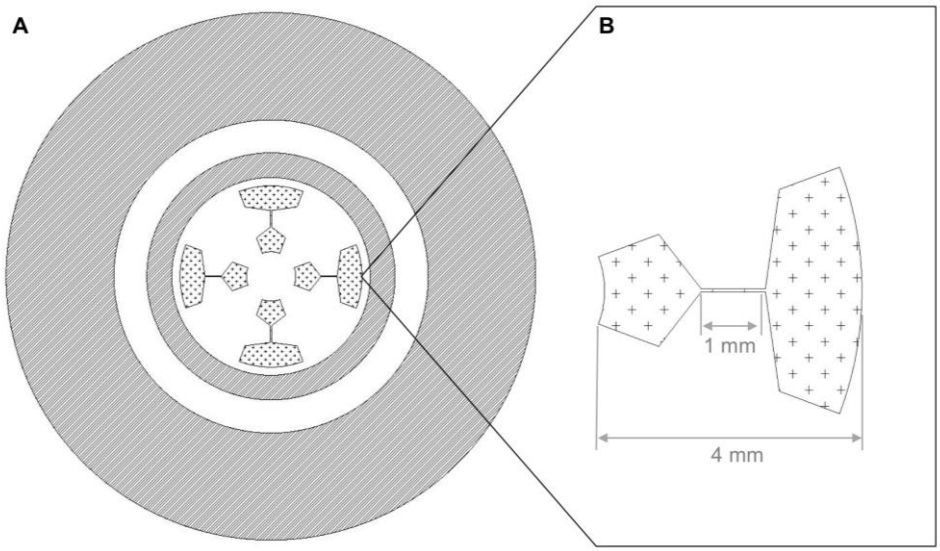

Figure 7. *Schematic illustration of the channel casted electrode structure for stretching characterization. Four dumbbell channel electrodes are positioned in the cell cultivation area of the pneumatic stretching systems (A). Single dumbbell electrodes (B) consist of two connection pads and the testing channel (l = 1 mm, w = 50 μm).*

3.2.3 Resistance Measurements

To characterize the properties of a fabricated thin-film electrode resistance measurements are commonly conducted [137]. Electrode resistance values allow conclusions about the conductivity as well as the structural integrity of an electrode material [137]. Resistance of the fabricated large electrodes was measured using a four-point (Keithley 2425 100 W Source Meter) probe set-up previously described in [138]. Due to area restrictions, the resistance of the patterned electrodes was measured using a multimeter (Fluke 175, Fluke Vertriebsges.m.b.H., Austria) in a two-point probe set-up. All measurements are conducted manually under dry contact between the electrode surface and measurement probe.

3.3 Piezoelectric Composite Membrane

In this section, the experimental design for an indirect electro-stimulative piezoelectric composite, utilizing CNC as active material is summarized. The introduced composite fabrication strategy results in irreversible surface embedment of CNC into a thin (d = 120 μm) PDMS membrane forming a PDMS-CNC composite membrane. Structural differences of a variety of casting methods, concentrations and pre-processing of the CNC solution were studied. Furthermore, the fabricated membranes were illustrative characterized in regards to their electro-stimulative functionality and integrable to the mechanical stretching device.

3.3.1 Cellulose Nanocrystals

Neutralized cellulose nanocrystals suspended in an aqueous solution were provided by Aalto University (Helsinki, Finland). Wood fibers recovered from birch bark were reduced to CNC through mechanical milling and chemical hydrolysis with sulfuric acid. After hydrolysis, a gel-like substance with a solid percentage of 2.36 % w/w nanowhiskers was formed. Finally, a neutral aqueous working suspension was obtained by suspending the acidic CNC-gel in a 0.5 sodium hydroxide solution. The CNC working suspension had an approximate solid content of 1.39 % w/w.

3.3.2 Fabrication of PDMS-CNC Composite Membranes

Requirements for the indirect electro-stimulative modular extension of the stretcher include that the added electrical component needs to be fully adhered to the cell cultivation area in order to allow direct transfer of mechanical strain from the PDMS membrane to adhered cells. Also, to transfer the piezo-electrically created charge to the cell layer, cellulose nanocrystals need to be concentrated at the membrane surface to come into direct contact with the cells.

Based on these requirements, a novel fabrication strategy for PDMS based nanocellulose composites was developed. The introduced process combines classical strategies used in nanocellulose composite fabrication: (1) the formation of CNC thin-films through direct deposition on a desired substrate and (2) polymeric reinforcement using CNC as filler material.

The developed fabrication process is schematically described in Fig. 8. It is based on a surface embedment strategy of CNC thin-films onto one side of the PDMS substrate. For the procedure, dry CNC thin-films are formed on a glass carrier. Hereby, CNC in an aqueous solution are casted onto the glass carrier. Due to consecutive solvent evaporation dry CNC thin-films are formed. The morphology and functionality of these CNC thin-films strongly depend on pre-treatment methods applied to the CNC solution prior to casting as well as the casting method itself. A variety of pre-processing and casting methods were conducted during this thesis work and are introduced in the following sections. After CNC deposition, un-cured PDMS is applied directly to the CNC thin-film permeating cavities formed between the cellulose nanocrystals. Partial embedment of the CNC thin-film in the PDMS matrix results in the formation of a functional composite structure. After curing, the resulting PDMS-CNC composite structure is simply peeled from the glass carrier.

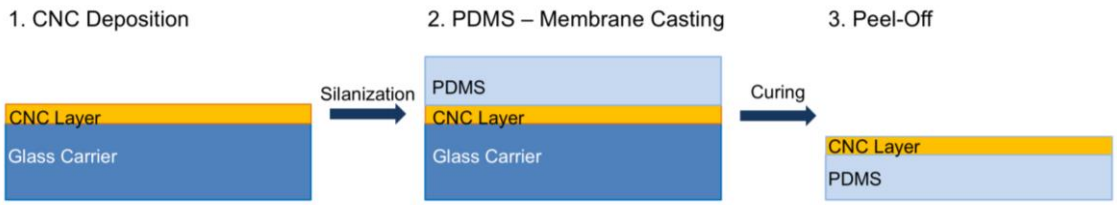

Figure 8. *Fabrication strategy for the embedment of crystalline nanocellulose into a thin, transparent PDMS membrane through a peel-off procedure.*

CNC thin-films were immobilized utilizing a variety of casting methods on a clean circular glass carrier (D = 100 mm, d = 2 mm). Hereby, 500 µl of CNC suspension are utilized unless otherwise stated. The resulting CNC thin-films were dried at room temperature in a protective environment (biosafety fume hood) for 10 – 20 min or unless completely dry.

The dry CNC thin-films on glass are placed in a desiccator together with 30 µl of Trichloro(1H,1H,2H,2H-perfluorooctyl) silane (Sigma-Aldrich Inc., USA) under applied vacuum (0.8 mbar) for five hours. This step reduced interfacial adhesion between PDMS and the glass carrier, which ensured easy removal of the PDMS-CNC composite membrane during peel-off [136], [139], [140]. Also, the treatment theoretically improved the interfacial cross-linking between the CNC thin-film and PDMS matrix by neutralizing OH-groups presented on the surface of CNC. Removing OH-groups on the CNC surface reduced the strong polarity of CNC. The non-polar PDMS matrix could then permeate the CNC thin-film much easier, leading to a more stable CNC-PDMS interfacial bond.

After silanization, a 120 µm PDMS layer was spin coated on top of the CNC thin film. The PDMS membrane was prepared using the standard protocol described earlier (see Section 3.1.1).After curing (10 h at 60 °C), the fabricated membrane was cut into circular pieces with a varying diameter (D = 25 – 32 mm) depending on the envisioned test. The resulting membranes were then manually peeled from the glass carrier and placed on a PS plate CNC embedded side facing upwards.

3.3.3 Casting Methods for Cellulose Nanocrystal Thin-Films

To study the structural variations of CNC thin-films on the glass carrier and PDMS-CNC composite membrane, four CNC casting methods were implemented and compared. Hereby, the previous described original CNC solution with a solid percentage of 1.39 % crystals was casted onto standard microscope slides (VWR, USA). Three parallel samples n = 3 were prepared for each casting method.

The four implemented casting methods were: (1) droplet casting, (2) roll casting, (3) dip coating and (4) spin coating. The utilized microscope slides were treated with oxygen plasma for 15 s at 30 W prior to material casting to enhance the wettability of the glass

surface and allow even material distribution. In drop casting, a V = 100 µl droplet of CNC solution was pipetted straight on the microscope slide and left until dry in a biosafety fume hood at room temperature. For roll casting, the microscope slide was slanted at a 45° angle. An CNC solution droplet (V = 100 µl) was allowed to roll down the so fabricated ramp leaving a trail of material on the microscope slide. The formed trail was allowed to dry at room temperature in a biosafety fume hood. Dip coating was achieved by slowly dipping the microscope slide, holding it vertical, into a beaker filled with CNC solution. The so coated slide, was placed in a vertical holder for drying at room temperature in a biosafety fume hood. Spin coating of the CNC solution utilized a three-step spin coating protocol: (1) 20 s at 200 rpm, (2) 30 s at 500 rpm and (3) 10 s at 100 rpm. After CNC deposition the substrate was left to dry in a biosafety fume hood as room temperature After drying, PDMS-CNC composite membranes were fabricated as described in Section 3.3.2 from all casted samples.

The morphology of the casted CNC thin-films as well as the PDMS-CNC composite membrane surface were visualized before PDMS casting and after membrane peel-off using the optical microscope described in Section 3.6. Hereby, phase contrast (PH) and differential interference contrast (DIC) methods at 200x total magnification were used.

3.3.4 Adhesion Analysis

The structural reliability of fabricated PDMS-CNC composite membranes strongly depends on the adhesion between the CNC and PDMS layer. Hence, a simple adhesion test set-up was utilized. It is to note that standard adhesion test methods are not compatible with the fabricated membrane structure as they require cutting the sample surface slightly [141]. As the available structure is too thin for such procedures, a simplified adhesion test was devised.

Droplet coated, dip coated and spin coated (500 rpm) PDMS-CNC membranes were stabilized on a PS plate with the CNC side facing upwards. Scotch tape was then pressed and flattened on the membrane for approximately 30 s. After the tape formed a reasonable adhesion to the membrane surface, it was removed in a rapid motion without damaging the membrane. This procedure was repeated up to three times on the same membrane area. The resulting membrane structure was optically characterized before and after the application of the scotch tape using a 200x total magnification.

3.3.5 Atomic Force Microscopy

Optical microscopes have a general maximal spatial resolution of 0.2 µm [142]–[144]. However, the resolution of optical microscopes depends also strongly on their hardware components, especially on the available objectives. The highest magnifying objective in the available optical microscope has a 20x magnification, hence limiting the system

in resolution. Nanocellulose crystals range in size dependent on their source and preparation method, but usually are around 0.1 - 1μm in length and 5 – 20 nm in width [145], [146]. Hence, especially at low CNC concentrations, optical microscopes are not able to visualize the structure of the fabricated membranes. Atomic force microscopes (AFM) can reach a lateral resolution of 30 nm and a vertical resolution of 0.1 nm, which makes them an optimal tool to visualize the crystal structure of the fabricated PDMS-CNC membranes.

The AFM XE-100 (Park Systems, USA) model was applied to image the crystal structure of CNC thin-films and PDMS-CNC composite membranes, which were not detectable in the optical microscope system. For illustration, a spin coated membrane and glass plate fabricated from 1.39 % original CNC solution at 1000 rpm were imaged. Imaging was done in non-contact mode with a standard ACTA AFM probe (AFMprobe, USA). Key imaging parameters are summarized in Table 1.

Table 1. *AFM Imaging Parameters*

Parameter	Value
Scan Size	3 μm
Frequency Set Point	1000 nm
Gain	1
Scan Rate	0.5 Hz

3.3.6 Pre-treatment of Cellulose Nanocrystal Solution

CNC easily form self-assembled structural clusters within an aqueous suspension [147] due to their chemical properties. This is mainly caused by the strong reactivity of the OH-rich crystal surface, which also promotes intermolecular binding of crystals through, for example, the formation of hydrogen bonds or Van-der-Waals forces [148][95] However, the piezoelectric sensitivity of a CNC suspension is reduced due to this cluster formation [114]. Hence, physical processing methods of the original CNC solution, aiming to reduce the size of formed clusters and ultimately achieving smoother membranes, need to be studied. In literature either sonication, centrifugation, or a combination of both treatments is used [95].

In order to compare the effect of pre-treatment of the CNC solution on the final PDMS - CNC composite membrane, centrifugation and sonication treatments of the original CNC solution were conducted. To ensure reliability of the comparison, studied PDMS-CNC membranes were fabricated utilizing the earlier described spin coating method

(see Section 3.3.3). However, to further study the influence of spin coating on the structural properties of a fabricated composite membrane, the second coating speed was varied. Spin speeds of 200 rpm, 500 rpm and 700 rpm were utilized.

The original CNC suspension was centrifuged (SL-8 Benchtop Centrifuge, Thermo Fisher Scientific Inc., USA) for 30 min at 4000 rpm and the resulting supernatant, containing a sample fraction of smaller crystals and crystal assemblies, was transferred into a fresh reaction tube. As the overall solid percentage of the solution dropped, due to the centrifuged fraction, the total weight percentage of the supernatant was determined by a scale comparison. Hereby, 1 ml of original CNC solution (m = 1.00305 g) was weighted on a microscale. Then, the weight of 1 ml centrifuged supernatant (m = 0.99526 g) was determined and the approximate percentage of weight loss calculated as the weight difference of the two samples. The centrifuged structure lost 0.78 % of solid content. Hence, the applied concentration of centrifuged CNC is 1.31 % w/w. Sonication of the original CNC solution was achieved using a tip sonicator (Soniprep 150Plus, MSE Ltd., UK) immersed into the solution. The solution was sonicated for 5 min at 10 % total amplitude whilst on ice. As no sample fraction was removed from the CNC solution, it retained the original concentration of 1.39 % w/w. All processed CNC solutions were used immediately after pre-treatment for PDMS-CNC composite membrane fabrication.

Furthermore, PDMS-CNC composite membranes from CNC solutions with lower solid content were fabricated. For that, the initial CNC solutions was diluted with distilled water to achieve a lower solid content. The resulting CNC solution concentrations of 1.39 %, 0.51 % and 0.06 % for untreated and sonicated CNC solutions as well as 1.31 %, 0.5 % and 0.05 % for centrifuged CNC solutions respectively were compared in their structural membrane capabilities.

In summary, the structural appearance of PDMS-CNC composite membranes fabricated from three pre-treatment solutions (original, centrifuged and sonicated), at three main spin speeds (200 rpm, 500 rpm, 700 rpm) and three concentrations (1.39 % and 1.31 %, 0.51 % and 0.5 %, 0.6 % and 0.5 %) per solution were compared. To ensure repeatability of the results, a total of three parallel samples (n = 3) per pre-treatment – spin-speed – concentration combination were prepared.

3.3.7 Piezoelectric Sensitivity Measurement

Piezoelectric sensitivity of PDMS-CNC composite membranes was characterized using a measurement set-up based on a mechanical shaker described earlier by S. Rajala et. al [94] The system functionality is briefly illustrated in Fig. 9. The applied mechanical shaker (Mini-Shaker Type 4810, Brühl & Kjaer, Denmark) generates a dynamic excitation force to the sensor by mechanical movement. The shaker generates a dynamic excitation force with force rating of 10 N sinusoidal peak and has a frequency range from DC to 18 kHz. A functional generator (AFG3101, Tektronix Inc., USA) provides a si-

nusoidal input signal for the shaker. Electrical charges generated by the tested material are amplified and compared to two highly sensitive commercial force sensors. A force sensor for the applied dynamic force (Model 209C02, PCB Piezotronics Inc., USA) and a load cell for the applied static force (Model ELFS-T3E- 20L, Measurement Specialties Inc., USA) were utilized as reference sensors in the measurement. Both sensing systems ensure that the measured sensor stays on the platform and regulate the range of excitation.

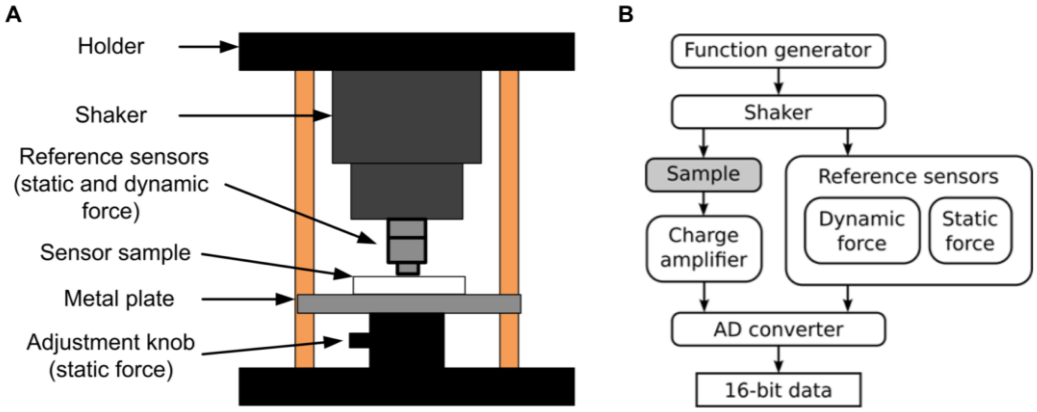

Figure 9. *Schematic of the testing set-up (A) and measurement set-up (B) of the piezoelectric measurement. In short, samples are mechanically stimulated using a shaker and the resulting piezoelectric sensitivity in [pC/ N] is measured. (Taken from* [24], [93]*)*

For piezoelectric sensitivity measurements, the PDMS-CNC composite membrane was sandwiched between two thin-film copper electrodes (d = 100 nm) evaporated on a polyethylene terephthalate (PET, Melinex ST506) film by e-beam evaporation (Model BC-3000, ACT Orion Inc., USA). As PDMS materials display high adhesion to smooth, surfaces no tape was needed to adhere the copper electrodes to the composite membrane. Fig. 10 illustrated the set-up of the measurement sensor. PDMS-CNC composite membranes were measured by using the copper electrode not facing the embedded CNC as measurement electrode, to catch the summarized effect of the membrane layer. Satu Rajala conducted all piezoelectric sensitivity measurements during the thesis work.

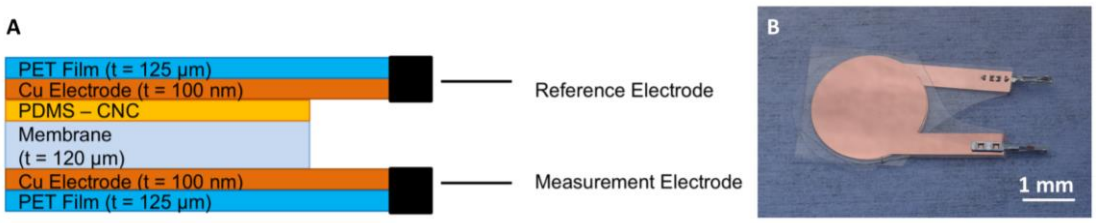

Figure 10. *Sensor design for piezoelectric measurements of PDMS-CNC composite membranes. Schematic drawing (A) and photograph (B) of the sensor set-up. (Adapted from[115])*

3.4 Evaluation of Biocompatibility

As the system is designed for applications in single cell and stem cell research, it is of high importance that the material used for the electro-stimulative component is compatible with biofunctionalization and cell cultivation procedures. Specifically, the applied material should not be toxic for cells by itself and be able to withstand aqueous cell cultivation conditions over an extended period of time [149]–[152]. Hence, this section describes a general cell cultivation test set-up to evaluate the biocompatibility of the developed electro-stimulative structures.

3.4.1 Protein Immobilization Procedure

Biofunctionalization procedures for nanomaterials aim to enhance the initial biocompatibility and functionality of the material [153][154]. Hereby, biomolecules, including proteins [155], peptides [155], [156] or fragments of genetic material [157], [158], are bound to a synthetic surface in a site-specific [159], [160] or random way [155], [161], [162] to form a continuous surface coating. This biofunctional layer should enhance cellular attachment and ultimately render initially non-biocompatible surface structures biocompatible.

PDMS is initially a biofouling material unfit for proper cellular attachment [76]. All electro-stimulative structures contain at least a fraction of PDMS in their surfaces. To study cellular attachment and growth behavior on the electro-stimulative systems, an unspecific protein coating protocol using physisorption is applied to all test surfaces.

To render PDMS [70] and PEDOT:PSS [163], [83] surfaces hydrophilic, and therefore compatible with biofunctionalization protocols, oxygen plasma treatments are commonly used. For the biofunctionalization protocol applied during this work, all samples were treated with oxygen plasma for 20 s at 30 W. Then, 250 µl of 0.1 % Gelatin (Sigma Aldrich Corp., USA) was applied to the test system and incubated for 1 h at room temperature. After protein incubation the system is washed rapidly three times with sterile phosphate buffered saline (PBS).

To study the surface coverage of the biofunctionalization procedure 0.1 % green fluorescence (Alexa Fluor 488) tagged Gelatin was adhered to the test surfaces in an identical procedure. Conjugated 0.1 % Gelatin was fabricated by using the commercially available protein labelling kit Alexa Fluor® 488 Protein Labeling Kit purchased from Thermo Fisher Scientific Inc. (USA).

3.4.2 Cell Type

Fibroblasts are an adherent mammalian cell type that, most commonly, can be found in inter-connective tissues [164]–[166]. This cell type is able to synthesize extracellular matrix components, such as collagen [164], [167]. Hence, their main function is to build the structural framework for mammalian tissues, which is especially important during wound healing. Due to their ECM synthesizing properties, they are commonly used in cellular research either as cells in a supportive feeder layer for stem cell cultivation and differentiation [42], [168]–[170], or as reliable and robust cell model for genetic research [171]–[173] and material testing [174]–[177].

Mouse embryonic fibroblasts (MEF) were obtained from Vesa Hytönen and Rolle Rahikainen (Tampere University, Tampere, Finland). However, the original cell sample was obtained from Wolfgang H. Ziegler (Hannover Medical School, Hannover, Germany). The cell line is a readily available line thoroughly characterized by E.D. Adamson et. al [178]. The MEF cells in this cell line contain a Vinculin protein knockout gene, which however does not affect cellular attachment and migration [5] important for biocompatibility testing.

The cells were grown in a T 25 cm^2 PET cultivation flask (Thermo Fisher Scientific Inc., USA) using a standard cell cultivation procedure [44], [127]. The cell culture was sustained using a culture medium based on a high glucose Dulbecco`s Modified Eagle Medium (DMEM, Thermo Fisher Scientific Inc., USA), which is free of sodium pyruvate and 2-[4-(2-hydroxyethyl)piperazin-1-yl]ethanesulfonic acid buffer. The medium was supplemented with 10 % fetal bovine serum (Thermo Fisher Scientific Inc., USA), 1 % penicillin / streptomycin (Thermo Fisher Scientific Inc., USA) solution and 1 % L-Glutamine (Thermo Fisher Scientific Inc., USA). Seeded cells were placed in a controlled culture environment (Incubator, Binder GmbH., Germany) for cultivation at 37 °C and 5 % CO_2.

3.4.3 Cell Cultivation – Biocompatibility Test

Cellular biocompatibility of PDMS-CNC composite membranes (CNC original 0.51 %, spin coated at 1000 rpm, n = 2) and channel casted Innophene electrodes (n = 2) were tested. As positive controls, pure PDMS membranes and standard PET culture wells were applied. Physisorbed 0.1 % Gelatin coatings were prepared as described in Section 3.4.1. on all samples (controls and samples).

For biocompatibility testing, MEF cells were seeded directly on the gelatin coated structures. Hereby, an initial cell concentration of 1200 cells / well (A = 1.13 cm^2) were seeded on each system. All systems were incubated and imaged (Magnification: 200x, Axio Observer.Z1, Carl Zeiss GmbH, Germany) after 1 h, 19 h, 27 h and 43 h of subculture.

3.4.4 Cellular Growth Characterization

Quantification of cellular growth is generally done by calculating the total cell number for each time point and presenting it in the form of a cellular growth curve to evaluate cellular attachment and biotoxicity of materials [44], [179]–[181]. The cellular growth curves were obtained for all samples. The number of living cells over a specific area at each sub-culture time point was manually counted from the optical microscope images using Fiji. Hereby, sample areas of A = 378266.6 μm^2 for 1 h and 19 h after sub-culture and A = 120000 μm^2 for 27 h and 43 h after subculture were counted. The total cell number per well was then estimated for the complete active cultivation area of 1.13 cm^2 per sample and plotted utilizing a logarithmic scale.

3.5 Optical Microscopy

Throughout the experimental process, the prepared surfaces were characterized with the help of an optical microscope system. The inverted optical microscope Axio Observer.Z1 (Carl Zeiss GmbH., Germany) was used in all experiments. This specific microscope was equipped with semi-automated control features controlling hardware, such as the camera shutter, exposure time, filter and objective turret as well as z-focus drive.

During image acquisition for this thesis, a variety of contrast methods were applied, including PH imaging, DIC imaging and fluorescence imaging. For fluorescence imaging, a wide range green fluorescence filter set was utilized (Filter Set 25 He, Carl Zeiss GmbH., Germany). Sample magnifications varied, but mainly objectives for 10x (A-Plan 10x/0.25 Ph1 M27, Carl Zeiss GmbH., Germany) and 20x (Objective LD A-Plan 20x/0.35 Ph2 M27, Carl Zeiss GmbH., Germany) were used, providing a total magnification of 100x and 200x respectively. The polarizing prism necessary for DIC imaging was only installed in the 20x objective, hence rendering this objective the magnification of choice for this method. The samples were imaged using a 1.4 Megapixel color camera (AxioCam MRc Series, Carl Zeiss GmbH., Germany) in black and white imaging mode and 50 % total light intensity. The system as functional unit is accompanied by the operational software Zen 2 (Carl Zeiss GmbH., Germany), which was used for image acquisition and initial post-processing.

3.6 Software

During the implementation of this thesis, different software packages were used, additionally to the device specific operation software modules, to obtain and process the accumulated data and prepare the illustrative figures.

General capabilities of the open source image processing software Fiji [128] were used to analyze and post-process the optical microscopy images obtained throughout the experiments and to prepare the figures. Hereby, especially contrast/ brightness balancing, filters (Sharpen, 1 pixel Gaussian Blur), region of interest manager and particle tracking were used. Additionally, for creating schematic figures, Inkskape (Inkskape Project, USA), Omnigraffle (The Omni Group, USA), Corel Draw X8 (Corel, USA) as well as Microsoft Power Point (Office for Mac, Mac OS X, Microsoft) were applied. Shown calculation results and charts were obtained using Microsoft Excel (Office for Mac, Mac OS X, Microsoft) and Origin Pro 6.1 (OriginLab).

4. RESULTS AND DISCUSSION

In this chapter, results of the experimental findings are discussed. In the analysis, fabrication and functional characterization of stretchable polymeric electrodes and PDMS-CNC composite membranes are discussed separately. For both materials, the fabricated structure, electro-stimulative functionality, stretchability and biocompatibility are demonstrated.

4.1 Functionality of Stretchable Electrodes Fabricated from Conductive Polymers

This section discusses structural integration of stretchable electrodes fabricated from a solution processable conductive polymeric ink (Innophene). The main results of the structural and functional characterization, presented in the following paragraphs, have been reported earlier by M. Viehrig et. al. [130]. Data taken from this publication is therefore not cited separately.

4.1.1 Thin-Film Electrode Characterization

Oxygen plasma treatment of PDMS substrates resulted in a low water contact angle (< 15 °) and therefore in high wettability of the substrate. This allowed the fabrication of homogenous Innophene thin-films on a cured PDMS membrane. The formed thin-films were highly transparent, but appeared light blue under normal room illumination.

It was possible to form large electrodes covering the complete circular cell cultivation area (D = 12 mm) using spin and spray coating. The formed thin-film electrodes display an optical transparency close to pure PDMS and are homogenous throughout the electrode area. Thus, they would allow live imaging of cells. Microscopy images of the resulting electrodes in comparison to pure PDMS can be seen in Fig. 11 (A, C). The resistivity of deposited electrodes was at 100 ± 10 Ω for spin coated electrodes and 80 ± 11 Ω for spray coated electrodes. However, upon release of the PDMS membrane form the PS plate during system assembly, cracking of the thin-film structures occurred. Crack formation, as illustrated in Fig. 11 (B, D), was observed throughout the complete electrode area limiting its optical properties for the envisioned applications, as light reflection on the formed cracks overshadows the remaining structure.

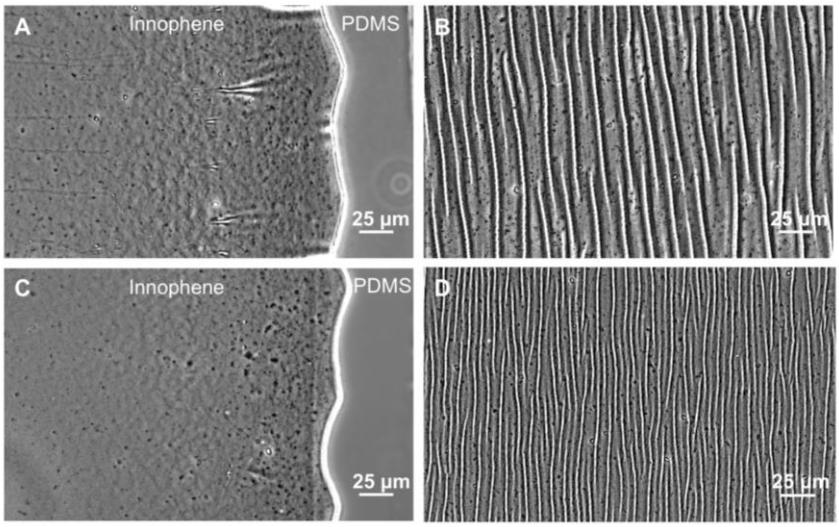

Figure 11. *Comparison of spray coated (A,B) and spin coated (C,D) Innophene layers before (A,C) and after (B,D) membrane release. (Adapted from* [130]*)*

Also, it can be expected, that crack formation represents areas with low interfacial adhesion between the PDMS substrate and Innophene. The risk of Innophene delamination and subsequent structural failure at those cracks can be classified as rather high. The observed cracks, however, could function as cellular guidance structures. Resistivity measurements of the cracked electrodes however revealed similar values compared to non-released membranes (deviation < 5 %). So the electrical functionality of the material layer was retained, while its mechanical function was lost.

The previously reported results suggest that the out-of-plane displacement of the membrane during substrate release exceeds the Young's modulus of the material, resulting in the observed crack formation. Therefore, with regard to the retained electrical functionality during membrane release, deposition methods applicable to a released substrate already incorporated into the final stretching device are expected to sustain the desired device properties. Spray coating and channel casting deposition methods can be applied also on the already assembled stretcher. However, the PDMS membrane in the assembled stretching system is already released and cannot be supported sufficiently for smooth surface application. By placing the stretcher on a rigid surface, air bubbles are captured below the PDMS membrane. These air pockets, cause the PDMS membrane to buckle and form local preliminary membrane strain variations, which need to be taken into account during Innophene deposition.

Hence, fabrication of large area electrodes, in the active membrane region of an assembled stretcher, by spray coating implied to be challenging. To avoid contamination of the system, the stretcher edges were partially covered. Due to this coverage, a small ring around the edge of the cultivation area could not be covered with conductive ink during spray coating. Also, the fabricated electrode was optically less transparent indicating a thicker layering of ink. However, optical microscopy imaging, as presented in Section 4.2, revealed a homogenously coated surface structure with sufficient transparency for

imaging. Resistivity of the resulting layers was 80 ± 11 Ω. Hence, the integration of spray coated electrodes to the assembled stretcher seemingly was a success. However, poor adhesion of spray coated electrodes illustrated in Fig. 11 suggests possible challenges during the application of mechanical strain to the coated PDMS membrane.

Channel casting of dumbbell channel electrodes by applying a small volume of ink to the center conduction pad was conducted successfully. Through capillary forces ink filled the testing channel and outer conduction pad evenly until the liquid levels were stabilized and Innophene crystallized. Optical images of the inner connection pad presented in appendix A, reveal smooth electrode layers with the highest transparency of all fabricated electrodes. Only at the channel edges, a slightly thicker material layer formed by meniscus forces could be observed. However, as this means more material is deposited at the channel edge, it can be seen as a positive effect as it possible stabilizes the adhesion between electrode and channel walls. Dumbbell channel electrodes showed a resistance of 150 ± 12 Ω measured between the conduction pads. Therefore, the patterned electrode exhibits superior optical and electrical functionalities compared to the other fabricated conductive polymer electrodes.

4.2 Equiaxial Stretching of Conductive Polymer Electrodes

Stretching characterization of conductive polymeric materials have generally been done for uniaxial [78] [94] [90], [138] or biaxial [182]–[184] stretching modes. Z. Bao et. al [78] reported that a basic PEDOT:PSS can withstand strains of up to 12 % without cracking in uniaxial stretching modes as well as that low strain values (< 30 % elongation) do not significantly change the resistivity of the material. Functionality tests of electrodes made from a conductive polymeric material under equiaxial strain have not yet been reported. Thus, we characterized the deposited electrodes under applied strain to verify the suitability of the material in equiaxial stretching.

Hereby, electrodes fabricated by spray coating on a free PDMS membrane displayed partial delamination of the electrode layer from the substrate as early as 1.25 % applied strain (vacuum pressure: 100 mbar). This is illustrated in Fig. 12 (A-D). During stepwise strain increase to 6.25 % applied strain (vacuum pressure: 250 mbar), the effect of partial delamination became increasingly apparent through heavy buckling of the electrode layer. Adhesion between the PDMS membrane and the ink seem to vary between positions and is not homogenous throughout the layer causing partial delamination. This results in the formation of various strain directionalities within the Innophene thin-film. Above 5 % applied strain (vacuum pressure: 200 mbar), the material did cause the substrate to exhibit cracking and functional loss. The resistivity of the electrode throughout the stretching procedure increased by 50 % from 80 ± 11 Ω to 120 ± 10 Ω. Hence, while the material retained its electrical properties, it experienced non-homogenous strain because of the partial adhesion. Varying strain fields caused by the non-homogenous ad-

hesion of the electrode also affected the PDMS substrate in a negative way. In Fig. 12 (E-H), the edge of the large electrode structure and non-covered PDMS membrane is shown. Until an applied strain of 2.5 % (vacuum pressure: 100 mbar) the PDMS membrane does not exhibit any type of change. However, also the electrode material itself is not moving with the applied strain, but rather the PDMS membrane below it. During linear strain increase to 10 % (vacuum pressure: 400 mbar) maximal strain, material fatigue of the PDMS membrane through the formation of stress cracks can be observed. The electrode moves with the direction of strain only in a minimal amount and exhibits massive edge delamination. This results in a functional failure of the system for the envisioned approach, as the mechanical stimulus applied by the membrane is not transferred to the electrode surface and delamination occurs.

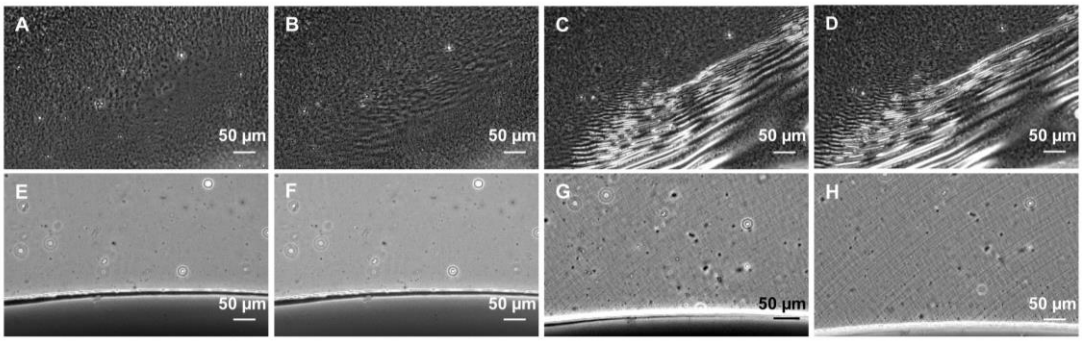

Figure 12. *Spray coated Innophene electrode on a released PDMS membrane integrated into the stretcher. In the electrode center (A-D) initial signs of delamination can be detected as ripple formation at 1.25 % (B) strain in comparison to the homogenous material layer at 0 % strain (A) occur. Throughout the strain increase over 6.25 % (C) to maximum strain (10 %, D) delamination effects become dominant. At the structure edge (E-H), no position change of the droplet could be observed between 0 % (E) and 2.5 % (F) strain. During strain increase the droplet positions shifts with the membrane slightly at 6.25 % (G) to maximal strain (10 %, H).*

Delamination of the electrodes fabricated by channel casting was initially observed starting from the channel edges at 3.75 % applied strain (vacuum pressure: 150 mbar). The effect continued along the channel side until the maximum strain of 10 % (vacuum pressure: 400 mbar) was observed. Figure 13 shows optical microscopy images of this process. Simultaneously, at 3.75 % applied strain, small cracks started to form within the electrode material. The electrode retained its electrical properties and only exhibited a 25 % increase in resistance from 150 ± 12 Ω to 200 ± 15 Ω. Delamination could only be observed at the sides of the channel as well as inside the reservoir and was not accompanied by buckling of the electrode material or signs of stress within the PDMS membrane, as illustrated in Fig. 13 and appendix A. Adhesion of Innophene ink to PDMS at the bottom of the channels seem to retain, while adhesion at the channel sides is low. But continuous delamination throughout repetitive stretching cycles could be observed, causing the electrodes to become loose and fixated only through the geometrical shape of the channel. In addition, the material also showed crack formation under equiaxial strain that limits the optical properties and therefore application potential for our envisioned platform.

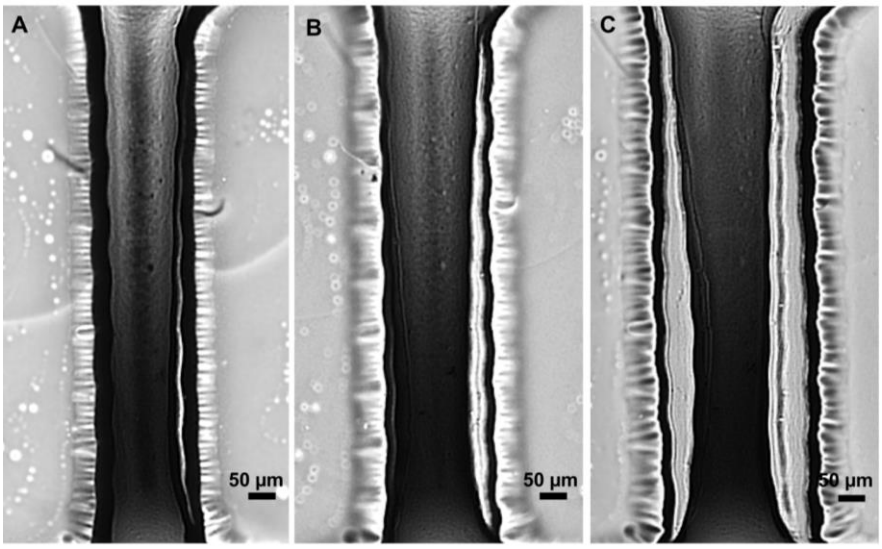

Figure 13. *Channel casted Innophene electrodes throughout stretching procedure. Delamination was first observed already at 3.75 % (B) strain at the structure edge. The delamination process continues along the channel edge throughout the applied strain curve, until at maximum strain (C) the channel edges were free standing.*

Throughout the stretching procedure both spray coated and channel casted electrodes retain their electrical functionality. Even after multiple stretching cycles, the measured resistivity returns to the measured initial values in resting state. Also no significant change in resistivity over time (> 2 weeks) in resting state could be detected. However, maximal peak resistivity values, especially in channel casted structures, could not be reached after the first stretching cycle due to delamination of the electrode material from the substrate.

4.2.1 Biocompatibility of Conductive Polymer Electrodes

For the applied graphene/ PEDOT:PSS, no biocompatibility test results were available at the preparation of this thesis. Therefore, biocompatibility tests based on cellular behavior were tested in a simplified set-up. Dumbbell channel electrodes were used as the test substrate, as they performed best during integration and functional testing and there is the highest chance that these structures will be applied in future electrode development.

The application of PEDOT:PSS and graphene based conductive inks in biomedical engineering, for example in fabrication of electronic skin [19-20], bioMEMS fabrication for electrical stimulation of neuronal cells [17] and thin film sensor fabrication for biosensing [22-25], have been sufficiently reported. Therefore, a general biocompatibility of the material can be expected. However, it is questionable if the systems would be compatible with surface biofunctionalization protocols for cellular attachment mediation

for conductive polymers [17]–[21] reported earlier. Due to the dumbbell channel electrodes, Innophene and pure PDMS surfaces are presented in the cell cultivation area.

MEF cells in a seeding cell concentration of 1200 cells/ well were applied to the cultivation chamber of the stretcher and cultivated for 43 hours. Cellular attachment and proliferation on the channel casted electrode structures and their surrounding PDMS structure were compared to a normally prepared stretching structure (smooth PDMS membrane).

As neither pure PDMS nor the conductive ink is initially supporting cell adhesion an unspecific biofunctionalization procedure was applied to all test membranes.

Fig. 14 illustrates optical microscope images taken throughout the cultivation period at 1 h, 19 h, 27 h and 43 h after sub-culture. MEF cells on a smooth PDMS membrane can be seen in row one. They exhibit good initial adhesion to the surface. The increasing amount of cells throughout the sub-culture period indicate normal cellular behavior. Also, only a low amount of dead cells could be observed in the culture. Cells grown on the channel casted structure (row two and three) however show a significantly different behavior depending on their location. Lower rates of initial cellular attachment seem to be apparent. Throughout the cultivation period, no significant increase of cell number were observed microscopically on the electrode material (row two) or surrounding PDMS structure (row three). Large numbers of dead cell could be observed especially in the structure center.

However, the channel casted electrode kept its structural appearance throughout the cultivation procedure. Hence, the system is in general compatible with the aqueous cell cultivation condition. Also the electrode structures allowed cell observation and single cell analysis supporting their structural suitability for integration into the stretcher. As additional feature, cracks formed in the electrode surface during the cell cultivation procedure functioned as cellular growth guidance structures.

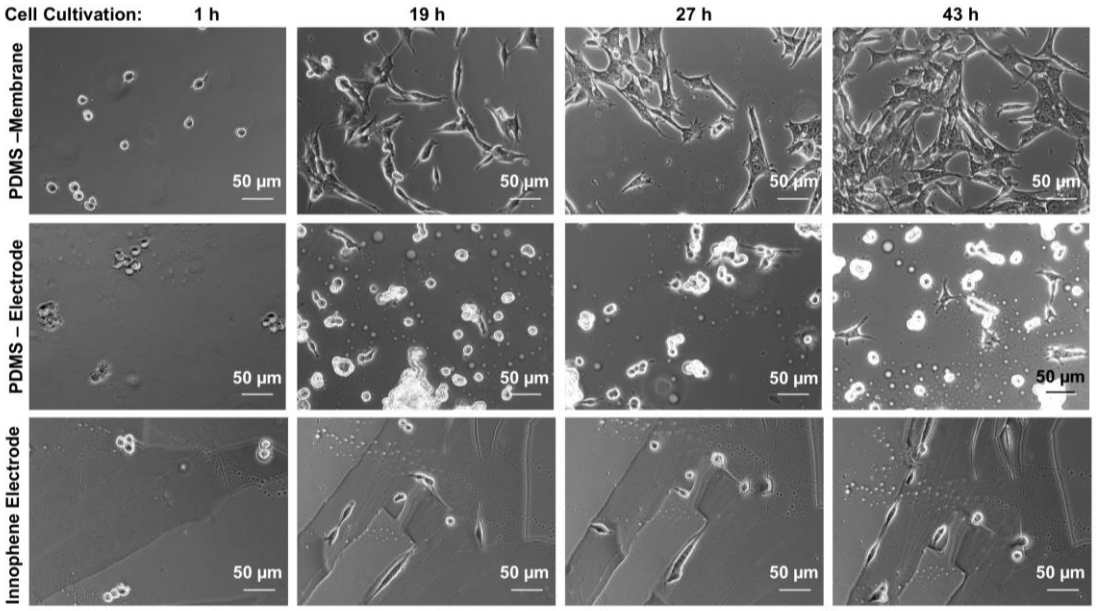

Figure 14. *MEF attachment and proliferation rates during a sub-cultivation period of 43 hours on varying materials. Cells cultivated on a 0.1 % Gelatin coated smooth PDMS control surface show average cellular attachment and proliferation rates. PDMS membranes with integrated channel casted Innophene electrodes (0.1 % Gelatin coating) show very limited cellular attachment and proliferation on PDMS as well as electrode sites.*

To quantify the biocompatibility of the systems, growth curves estimating the development of cellular numbers over the cell cultivation period were prepared. In Fig. 15, growth curves of cells cultured on smooth PDMS controls as well as free PDMS and electrode surfaces on channel casted structures are shown. The curves show that the development of cellular numbers over the cultivation period goes in a slower rate on the channel casted structure compared to pure PDMS membranes.

Cell numbers on pure PDMS develop in a standard growth curve [44] reaching a cell concentration of 85 500 cells/ well. This is in the normal cellular development range for a nearly confluent single cell layer. [44] During initial cell attachment (lag phase), cell numbers drop by 20 % compared to the initially seeded concentration, due to the fact that not all seeded cells remained viable or attached to the membrane. Cell numbers then increase exponentially during cell cultivation.

For channel casted structures, only a maximal cell concentration of 20 000 cells/ well on electrodes and 17 000 cells/ well on PDMS was achieved, which is significantly lower compared to the control structure. During initial attachment, cell concentrations dropped about 70 % on the electrode surfaces and 40 % on the surrounding PDMS. However, still an increase of cellular numbers over time could be observed indicating that the cells stayed viable during the cultivation period. As previously reported, MEF are ECM producing cells. They fabricate their own ECM matrix after initial attachment to a surface.

So the prepared channel casted surfaces were not initially suitable for cellular attachment. However, a small margin of cells stayed attached to the structure and produced their own ECM proteins, resulting in a slower proliferation rate. These result indicate an initial biocompatibility of the electrode surface and surroundings. However, the applied biofunctionalization procedure apparently was not sufficient.

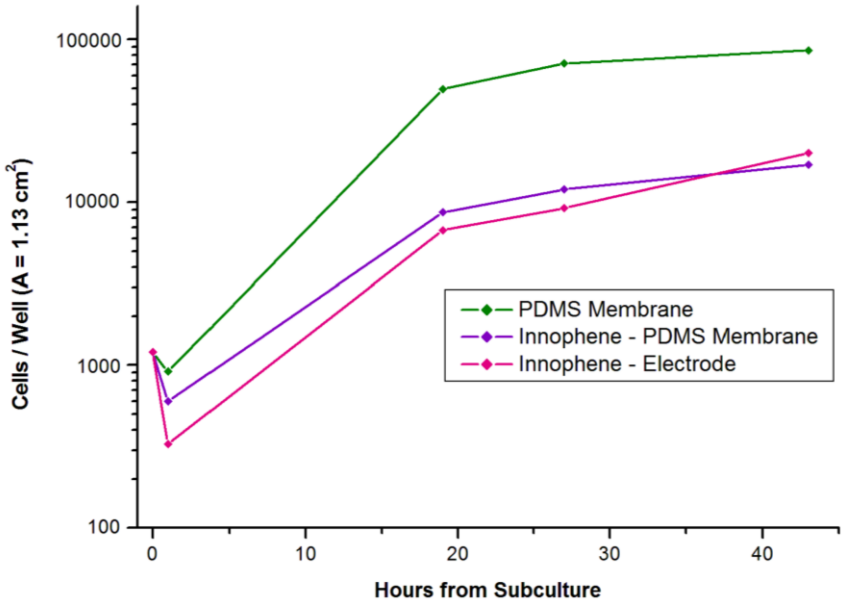

Figure 15. *Growth curve of MEF cells cultivated on pure PDMS and channel casted electrode structures (on top, next to electrode). The total cell number at 43 hours of subculture at the control PDMS membrane is 10-fold higher than the achieved total cell number at PDMS membranes including channel casted Innophene electrodes. Also an initial drop of cell number at 1 hour of subculture indicates attachment challenges.*

To further illuminate the previously achieved results, the surface functionalization procedure was repeated on a new system with fluorescence tagged Gelatin. Fig. 16 illustrates the distribution of Gelatin over the surface through fluorescence microscopic images on all surfaces. On the pure PDMS membrane surface (A), a homogenous protein coverage was achieved. However, PDMS surrounding the dumbbell channel electrodes (B) show a patch attachment of Gelatin and no protein was bound to Innophene electrodes (C). Over the complete stretching structure, an only partial covered surface is presented for protein attachment. This leaves layers vulnerable for partial protein detachment during the washing step resulting in non-homogenous coated surfaces. Hence, more complex biocompatibility strategies compatible with a material mix need to be applied on the fabricated membrane. M. Morzocchi et. al [185] suggest that cellular attachment of PEDOT:PSS substrates is mediated by either reduction or oxidation of the surface. The choice of process strongly depends on the individual cell line. Results suggest that MEF cells on PEDOT:PSS based materials need a reduced electrode surface for cell cultivation.

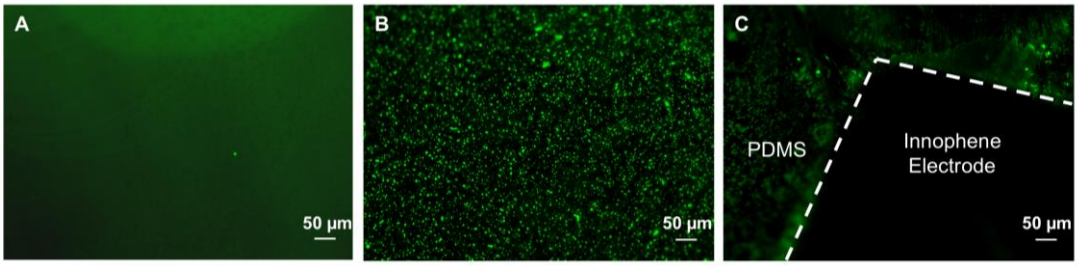

Figure 16. *Fluorescence images of a pure PDMS membrane (A) and a PDMS membrane (B) including channel casted Innophene electrodes (C) coated with 0.1 % fluorescence tagged Gelatin. Pure PDMS expresses a homogenous fluorescence signal, while the membrane of electrode integrated structures has an in-homogenous, spot-like signal. No fluorescence signal was obtained from the Innophene electrodes.*

4.3 Functionality of Cellulose Nanocrystals

A novel fabrication strategy for prototyping a PDMS-CNC composite membrane by surface material embedment of piezoelectric CNC is discussed in this section.

4.3.1 Structural Analysis of Nanocellulose Composite Membranes

There are three main strategies known for the fabrication of CNC nanocomposite material: (1) enforcement of polymeric materials through suspension of dry CNC in the polymer matrix, (2) CNC thin-film fabrication on various substrates from aqueous solution, and (3) electrospinning of CNC based materials.

In the experimental section of this work, a novel fabrication strategy for PDMS-CNC composite membrane through structural embedment of CNC thin-films into a PDMS matrix is introduced. Hereby, the fabrication strategy for the applied CNC thin-film can be easily varied, while other fabrication steps remained the same. Hence, combining classic fabrication strategies (1) and (2) to achieve a novel geometry for integration into the mechanical stretcher. In the following sections, a variety of CNC thin-film preparation methods are compared in regards of the resulting PDMS-CNC composite membrane morphology.

Comparison of Cellulose Nanocrystal Thin-Film Casting Methods

Fig. 17 illustrates CNC thin-films and resulting PDMS-CNC composite membranes prepared by four casting methods. The casting methods of choice are: (1) drop coating, (2) dip coating, (3) roll coating and (4) spin coating. All applied casting methods have in common, that optically visible, homogenous CNC thin-films were successfully integrated into the PDMS membrane surface during composite fabrication. Fabricated PDMS-CNC composite membranes are apparent morphological duplicates of the original CNC thin-films. Their surface morphology is directly transferred during peel-off to the PDMS membrane.

Also, as shown in the third column of Fig. 17, CNC thin-films were only partially transferred through the peeling procedure, leaving mostly continuous films on the original glass carrier. The only apparent difference between the surfaces is their distinctive morphology, which depends on each specific casting method applied.

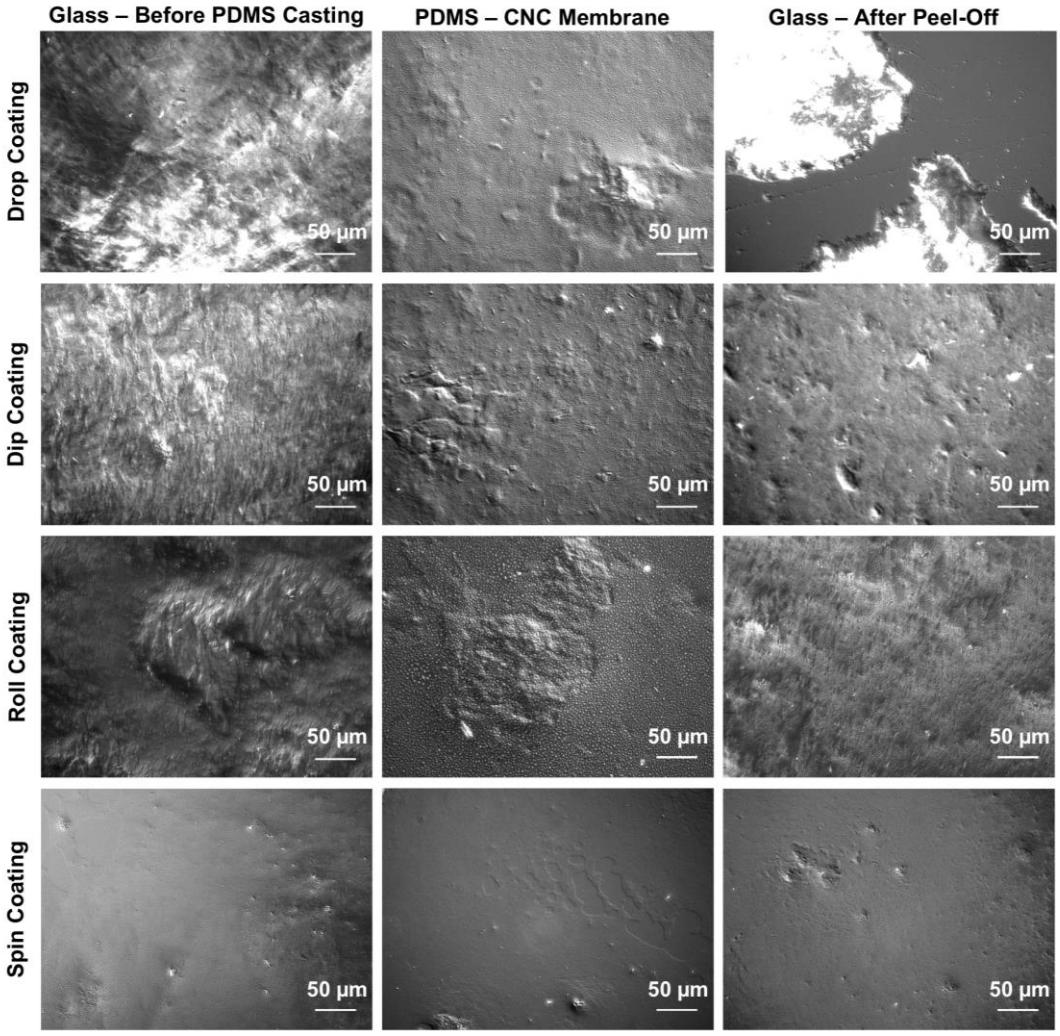

Figure 17. *Optical comparison of resulting CNC layers prepared through a variety of casting methods. CNC deposited on glass was visualized before and after molding and peel-off. Also corresponding PDMS-CNC composite membranes are presented.*

Droplet casting of CNC thin-films results in rough surfaces with apparent height variations on the glass carrier. Due to the drying procedure, concentric ring structures form over the surface resulting in large height differences. In the corresponding PDMS-CNC composite membrane, small regular spot structures, that do not correspond to the original CNC thin-film could, be observed. These structures have formed after PDMS casting and cannot be observed on the CNC thin-films after peel-off. Hence, these structures are most likely caused by the PDMS casting procedure itself. During PDMS casting, the liquid polymer permeates cavities between the crystals of the CNC thin-film. PDMS seeps through a majority of the layer to achieve CNC embedment. This indicates, that only thin-film areas saturated with PDMS bulk solution are transferred to the composite

leaving remaining CNC layers on the glass substrate after peel-off. Hence, the intramolecular forces formed within the CNC thin-film are weaker than strain applied by the peel-off procedure, resulting in only fully embedded CNC crystals to be transferred to the composite membrane. As for why PDMS does not reach fully permeate the CNC thin-film, this is probably caused by the spin coating procedure applied during fabrication of the PDMS membrane. Only a thin PDMS film is applied to the CNC surface and immediately after deposition placed in an oven for curing. During curing, long polymeric chains are created and the material becomes a rubber-like consistency. So depth of permeation can be linked to the curing time and material thickness, as apparently only a fraction of the CNC thin-film is fully embedded in the PDMS matrix before the viscosity of the PDMS matrix becomes too high.

Dip coated and roll casted CNC thin-films express a similar roughness as droplet casted structures. Surface layer morphology follows forces applied through the casting procedure (e.g. downwards force through gravity). This causes layering of CNC in the thin-film. The resulting membranes are rather thick and largely structured through this material layering. Also, the earlier described spot areas resulting from PDMS casting can be observed. PDMS spot sizes in roll coated composite membranes is larger compared to dip or droplet casted membranes, in which they are nearly not optically visible. Apparently, CNC networks formed by roll coating have larger intrinsic crystal distances resulting in a more porous network.

Spin coated CNC thin-films on the other hand express a smooth, homogenous layer with smaller height differences compared to the other structures. Also no PDMS spots are optically detectable, which indicates a tightly packed CNC layer. In regards to the envisioned functionality, a tightly packed layer is regarded as beneficial, as it ensures a homogenous transfer of electrical charges throughout the membrane.

Atomic Force Microscopy

Dimensions of single nanocellulose crystals are below the maximal resolution achieved with an optical microscope. However, accumulations of nanocellulose crystals during material casting can be optically observed due to the formed CNC thin-film as illustrated the previous section. To study crystalline structures of CNC, higher resolution images are necessary.

Figure 18 presents atomic force microscope images of CNC thin-films originally deposited on glass (A) and the resulting PDMS-CNC composite membrane (B). The applied layers were fabricated by spin coating with high speed (1000 rpm) from an untreated 1.39 % CNC suspension. The achieved images suggest, that a sufficient amount of nanocellulose crystals was transferred from the glass carrier to the PDMS-CNC composite membrane. Crystals displayed an average diameter of 7 – 8 nm and are around 100 nm in length. This crystals morphology was not changed during the composite fabrication procedure retaining the functional capabilities of CNCs.

As no crystal orientation procedure was applied during film formation, deposited layers display a random crystal orientation. Hence, the functionality of the achieved composite is determined by the casting method and resulting structure of the CNC layer.

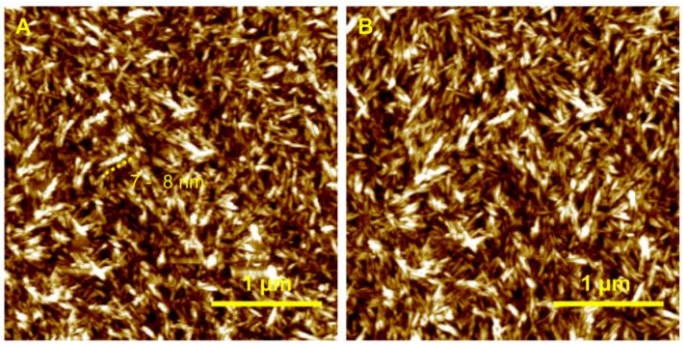

Figure 18. *Atomic force microscopy images of CNC layers on glass (A) and the resulting PDMS-CNC composite membrane (B). CNC layers on glass were prepared by spin coating at 1000 rpm followed by PDMS molding for composite fabrication.*

Layer Adhesion

Mechanical stability of the formed PDMS-composite membrane is of high importance for the functionality of the stretcher. Detachment of CNC layers during cell stimulation will cause mechanical and functional failure of the system, as the stability of the composite membrane is reduced and less electro-stimulative elements are present.

Previously obtained results suggest (see previous section) that the porous crystalline cellulose network formed through a variety of casting methods is fully surface integrated into the PDMS membrane. However, at the interfacial surface between CNC and cell cultivation area cellulose nanocrystals might be only partially covered by the PDMS matrix. Freeing of CNC during stretching could cause functional failure and, in worst case, cellular detachment.

In appendix B PDMS-CNC composite membranes fabricated through different casting methods before and after adhesion testing using scotch tape are illustrated. No disturbances of the CNC layer integrity could be observed in any of the casting methods. The chosen adhesion test method only added unspecific particles (dust) to the membrane instead of detaching significant amounts of cellulose nanocrystals. Hereby, neither the roughness nor the thickness of the composite layer did influence crystal adhesion, rendering the influence of different casting methods on the PDMS-CNC composite membrane interfacial adhesion insignificant.

Influences of Pre-treatment of Cellulose Nanocrystal Solution

Nanocellulose crystals suspended in an aqueous solution tend to form structural nanoclusters held together by strong inter-molecular bonds. A variety of physical treatment procedures for CNC suspensions have been introduced in order to separate such nanoclusters and study the functional properties of separated nanocellulose crystals [95]. Centrifugation and sonication have been the most popular treatment methods [95]. Hence, the effect of both pre-treatments on the morphology of fabricated nanocomposite membranes need to be studied.

Other possible influences during CNC thin-film fabrication is the concentration of the CNC suspension applied. Dilution of the original solution is expected to cause reduced layer thickness in the CNC thin film. Furthermore, as reported earlier in this thesis spin coating is the casting method of choice for CNC thin-film fabrication. Final layer thicknesses in this method are determined by the applied spin speed. Hence, spin speed variations were taken into account.

Fig. 19 compares PDMS-CNC composite membranes fabricated from the original CNC suspension (A), centrifuged CNC suspension (B) and sonicated CNC suspension, taking into account variations in concentration and spin speed.

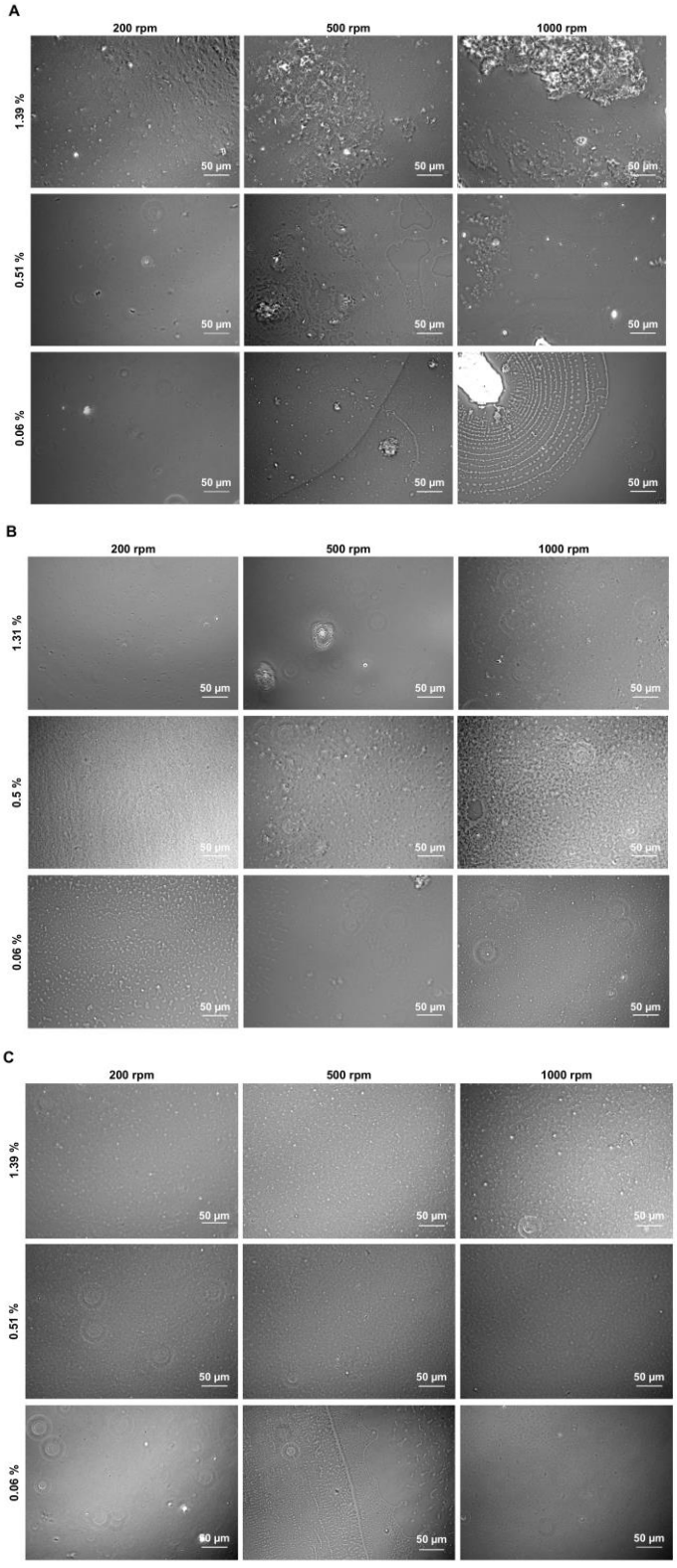

Figure 19. *PDMS-CNC composite membranes fabricated from the original untreated CNC suspension (A), centrifuged CNC suspension (B) and sonicated CNC suspension (C) using spin coating. The effect of varying concentrations and spin speeds on the structural integrity of the membrane coverage can be observed.*

Composite membranes fabricated from the original CNC solution show reduction of layer thickness in CNC thin-films with increasing spin speed and concentration, as the originally homogenous layer becomes non-homogenous. Application of the original CNC solution at 1.39 % resulted in irregular layers including large height differences and visible cluster formation, while at a concentration of 0.51 % only small clusters remained and at 0.06 % layers became nearly non-detectable. PDMS-CNC composite membranes prepared at 0.06 % and 1000 rpm expressed cavities in the CNC thin-film surrounding single clusters. Optimal processing parameters for the fabrication of smooth, homogenous composite membranes, that are optically detectable, can be found between 0.51 % at 200 - 1000 rpm and 0.06 % at 200 – 500 rpm.

Centrifugation of the original CNC suspension removes large particles and CNC cluster aggregates from the suspension, resulting in a more homogenous surface coverage. Composites fabricated with 1.31 % and 0.5 % suspensions mostly exhibit optical detectable homogenous surfaces. Only the 0.5 % composite membrane fabricated at 1000 rpm contained small cavities and therefore is not representing a homogenous surface coverage. Composite membranes fabricated from 0.06 % suspension all appeared to have a non-homogenous CNC thin-film containing cavities.

All resulting PDMS-CNC composite membranes fabricated from the sonicated CNC solution were barely detectable by optical microscopy. Composite membranes prepared from 1.39 % and 0.51 % suspension over the full range of spin speeds show homogenous layer characteristics. At 0.06 % non-homogenous composite layers are formed throughout the spinning parameters. However, large spots indicating PDMS permeation became optical apparent. Hence, it can be assumed that the method resulted in the formation of a non-homogenous CNC thin-film in regards to CNC crystal distribution. As a result, the density of composites fabricated from sonicated CNC suspension becomes questionable in regards of functionality.

The structural conformation of PDMS-CNC composite membranes highly depends on the pre-treatment parameters applied during CNC thin-film fabrication. Optimal PDMS-CNC composite membranes include a homogenous, dense CNC layer, which can be obtained with a wide variety of pre-treatment parameter sets. Also crystal densities should be reasonable high and optically traceable for control purposes. Evaluating the results in regards to these criteria, PDMS-CNC composite membranes fabricated from a centrifuged CNC suspension starting from 0.5 % concentration are slightly superior in regards to surface morphology.

However, this analysis was purely based on optical imaging results. Data from thickness measurements of the CNC films and higher resolved imaging technologies need to be conducted in order to give a more quantitative conclusion.

4.3.2 Functional Analysis of PDMS-CNC Composite Membranes

The envisioned electromechanical stimulation system for stem cell research sets a range of requirements on the functionality of the developed structure. Hence, it is of high importance to thoroughly characterize the developed composite membrane to access its system compatibility. This thesis covers preliminary functional analysis of required mechanical, electrical and biological functionalities.

Piezoelectric Effect

Overall piezoelectric sensitivity values for spin coated composite membranes under varying processing parameters (spin speed, concentration), fabricated from the original CNC suspension, are summarized in Table 2. Measured average piezoelectric sensitivity of composite membranes ranges from 8 – 11 pC/N. PDMS references expressed an average piezoelectric sensitivity between 0.5 – 1.5 pC/N. The difference between the materials is significant, which indicates that the embedded CNC are reacting actively to the applied mechanical strain. PDMS-CNC composite membranes show piezoelectric sensitivity above reported values for cellulose nanofibrils (5 -7 pC/N [115]) , but below PVDF (d_{33} = -33 pC/N [116]).

Table 2. *Piezoelectric sensitivity values of PDMS-CNC composites membranes fabricated from the original CNC solution.*

Electrode	1.39 % Sensitivity [pC/N]	0.51 % Sensitivity [pC/N]	0.06 % Sensitivity [pC/N]
200 rpm	8.02 ± 2.82	19.74 ± 7.80	6.13 ± 5.70
500 rpm	0.57 ± 0.51	11.12 ± 1.14	11.52 ± 3.17
1000 rpm	9.88 ± 0.98	9.33 ± 2.15	2.13 ± 0.95

Table 3 illustrates overall piezoelectric sensitivity values for PDMS-CNC composite membranes fabricated from the centrifuged CNC solution. Measured average piezoelectric sensitivity of composite membranes ranges from 5 – 10 pC/N. PDMS references expressed an average piezoelectric sensitivity between 0.5 – 1.5 pC/N. In comparison to the PDMS references PDMS-CNC composites fabricated from centrifuged CNC express a clear piezoelectric response to mechanical strain. However, the average piezoelectric sensitivity of composites fabricated from centrifuged CNC solution lies slightly below the one for PDMS-CNC composites fabricated from the original CNC solution. It corresponds more to the piezoelectric sensitivity of CNF films (5 -7 pC/N [115]).

Table 3. *Piezoelectric sensitivity values of PDMS-CNC composites membranes fabricated from centrifuged CNC solution.*

Electrode	1.31 % Sensitivity [pC/N]	0.50 % Sensitivity [pC/N]	0.05 % Sensitivity [pC/N]
200 rpm	1.55 ± 0.91	4.13 ± 0.45	5.50 ± 0.76
500 rpm	0.96 ± 0.16	9.86 ± 2.04	7.00 ± 2.06
1000 rpm	5.25 ± 2.27	6.75 ± 1.70	15.91 ± 12.70

The average standard deviations of PDMS-CNC composite membranes obtained from a centrifuged CNC solution lies in general below the one for nanocomposite membranes obtained from the original CNC solution. This can be explained with the surface morphology of the obtained nanocomposite surfaces. PDMS-CNC composite membranes include large CNC cluster structures. During the measurements, areas with a higher amount of CNC (cluster) express higher piezoelectric sensitivity values compared to smooth areas. Hence, in average, a larger average standard deviation can be observed. The homogenous surface morphology of PDMS-CNC composite membranes obtained from the centrifuged CNC solution leads to a lower average standard deviation compared to composite membranes fabricated from the original CNC solution. However, in both cases the average standard deviation differs still largely. This can be explained by the measurement set-up. The composite membranes were directly sandwiched between the copper electrodes. Hereby, there is a high possibility to enclose air bubbles between the membrane and copper electrode surface. These air bubbles accord for an unstable connection between the electrode and composite substrate, leading to a higher variation in the piezoelectric sensitivity.

The achieved values represent a measurable piezoelectric sensitivity, which is a sufficient indication for the functionality of the structure. However, only non-oriented crystalline nanocellulose were utilized during the experimental procedures. It can be expected that higher degrees of orientation result in higher sensitivity values.

The piezoelectric properties of a PDMS-CNC composite membrane strongly depend on the fabrication procedure. This becomes apparent, as the obtained piezoelectric sensitivity values for varying pre-treatment and CNC thin-film processing conditions correlate with the optical analysis conducted in the previous section. Deposited CNC thin-films expressing a smooth, homogenous, coating in the optical detection range show higher piezoelectric sensitivity than non-homogenous, rough coatings that contain CNC clusters or other irregularities on the surface. So the piezoelectric sensitivity of a PDMS-CNC composite membrane is strongly related to its structural properties caused by pre-treatment and casting method of the CNC thin-film.

Strain Analysis

The pneumatic cell stretching device developed by J. Kreutzer et. al [13] can achieve a maximal static in-plane strain ε_P of 9.5 % ± 0.3 % [13] at a partial vacuum pressure of 392 mbar. As the functionality of the original mechanical stimulation system should not be majorly altered by the electro-stimulative modular extension, it is of high importance to also take the stretchability of the module into account. Fabricated PDMS-CNC composite membranes show promising structural integration capabilities and functionality. However, cellulose nanocrystals are very brittle materials [186]. As relatively large amounts of CNC are integrated into the membrane surface, it can be expected that the overall system stretchability should is reduced leading to a loss of mechanical stimulative function.

The maximal static in-plane strain of a PDMS-CNV composite membrane fabricated by spin coating (c = 1.39 %, 500 rpm) from the original CNC suspension was calculated. The PDMS-CNC composite membrane has a maximal in-plane strain of 9.5 % ± 2.9 % at 392 mbar. Surface embedment of CNC thin-films into the PDMS membrane does therefore not reduce stretchability of the membrane. In accordance with the adhesion tests and optical characterization of the composite structure, it can be assumed that a sufficient amount of PDMS permeated into the cavities between the separate cellulose nanocrystals to sustain overall stretchability of the membrane

However, strain variation between landmarks is with 2.9 % significantly higher than the maximal strain deviation of 0.3 % in the original stretcher. The maximal strain was calculated by comparing a total of 10 particle trajectory landmarks per sample (n = 3). Therefore, a larger active area per sample is covered leading in the possibility of higher displacement variations between landmarks. Another explanation for this large deviation lies in the nature of system assembly. In the original stretcher, the flexible PDMS membrane is bonded to the stretcher body while being supported by the PS plate used during the casting process. Hence, the membrane is only released from the substrate after system assembly. This is not possible with the composite membranes, as they need to be released from the CNC substrate and flipped prior to stretcher assembly. As this is a manual procedure, the it cannot be fully guaranteed that the composite membranes are placed perfectly flat on the intermediate support. During placement, small air pockets can be formed or the membrane is intrinsically strained resulting in local variations in final strain response.

4.3.3 Biocompatibility of Nanocellulose Membranes

Evaluating the biotoxicity of crystalline nanocellulose surfaces has caused a controversial discussion since introducing the material [99]. Depending on the study conditions, CNC materials were classified as toxic, non-toxic but not enhancing cellular properties, or biocompatible with cell cultivation experiments.

However, the highly reactive surface (OH-groups) of CNC make them a well suiting material for biofunctionalization procedures of all kind. Due to the native hydrophobicity of the PDMS membrane applied in the original stretcher, an unspecific biofunctionalization procedure based on physisorption of extracellular matrix proteins is used to mediate cellular attachment [13]. Therefore, biocompatibility testing of PDMS-CNC composite membranes was done using a similar functionalization procedure.

Fig. 20 shows optical microscope images of MEF cellular development throughout a cultivation period of 43 hours on different substrates. Cellular attachment and proliferation on PDMS-CNC composite membranes were compared to pure PDMS membranes and a standard cultivation well. Optical comparison of the cultivation substrates reveals only a minor difference in cellular behavior between the substrates. Initial cellular attachment appears to be stronger in PDMS-CNC composite membranes compared to the control surfaces. Cells cultivated on the composite surface express a high number of elongated cell morphologies already after one hour of cultivation. This cellular behavior is a strong indicator for an easier cellular attachment. Proliferation rates of cells throughout the period of sub-culture (43 hours) seem similar. After 43 hours nearly confluent single cell layers could be observed on all three test surfaces.

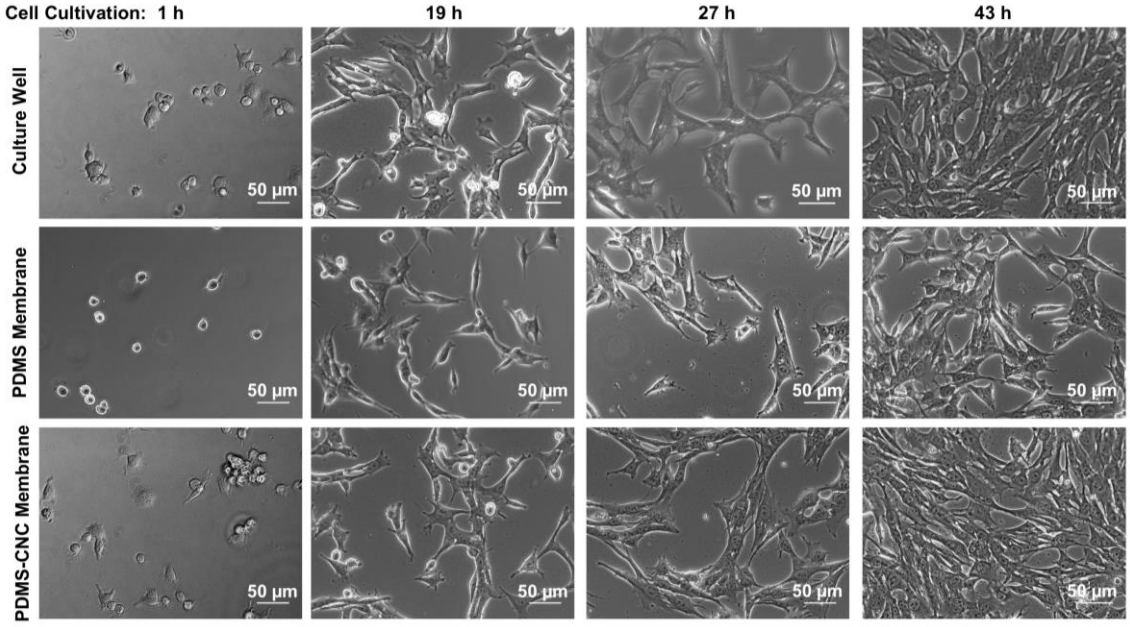

Figure 20. *MEF attachment and proliferation rates during a sub-cultivation period of 43 hours on varying materials. Cells cultivated on a 0.1 % gelatin coated standard culture well and smooth PDMS control surface show average cellular attachment and proliferation rates. PDMS-CNC composite membranes (0.1 % gelatin coating) show enhanced cellular attachment at 1 h beginning of subculture.*

Growth curves, demonstrating development of living cell numbers per culture area throughout the cultivation period, for all substrates are shown in Fig. 21. The obtained growth curves show a classical behavior. After cellular attachment (lag phase), cell numbers grow exponentially throughout the cultivation period. During lag phase cell numbers on pure PDMS and classic culture wells drop by approximately 20 %. This is a quite normal behavior, as not all initially seeded cells (1200 cells/ well) remain viable throughout cell seeding and attachment. However, total cell numbers on PDMS-CNC composite membranes did not decline during the same period. Hence, exponential cell growth already started at this point in cell cultivation mediated by a faster attachment process. Commonly, cells prefer slightly rough surfaces, such as the utilized PDMS-CNC composite membrane, to smooth surfaces, such as PDMS. The crystalline structure of the composite surface provides sufficient anchor points for cells to attach resulting in a faster and stronger cellular attachment procedure. However, during further cell cultivation growth curves show similar behavior. At 43 hour of sub-culture, PDMS-CNC composite membranes contained approximately 110 500 cells/ well, pure PDMS membranes 85 500 cells/ well and the culture plate 142 300 cells/ well. All concentrations are acceptable for a nearly confluent membrane, even so pure PDMS surfaces are lacking slightly behind the culture well and composite membrane.

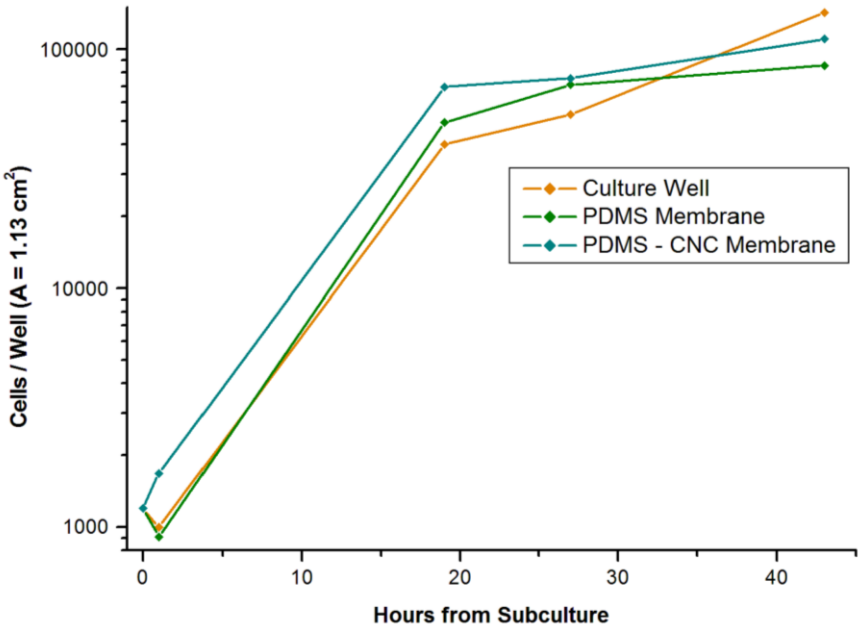

Figure 21. *Growth curve of MEF cells cultivated on standard culture well, pure PDMS and PDMS-CNC composite membrane structure. The total cell number at 43 hours of subculture show no significant (<5 %) difference. PDMS-CNC composite membranes show enhanced cellular attachment at one hour and increased cell numbers at 19 hours after subculture.*

5. CONCLUSION

Two distinctively different concepts for integrating an electro-stimulative component in an existing equiaxial mechanical stimulation device were shown. Component integration and functionality on a stretchable substrate was studied as key factors for the envisioned biomimetic cell culture device application.

The applied graphene/PEDOT:PSS ink is initially compatible with cell cultivation conditions, as it is water soluble and non-toxic. Fabricated electrodes display features of material fatigue (e.g. crack formation) already at low equiaxial strains, which stands in contrast to previously reported strain values in uniaxial and biaxial strain modes. On the other hand, the electrical properties of the material were retained before, during and after stretching, which makes them a material with great potential for the envisioned application, given different integration procedures. General biocompatibility and compliance with cell cultivation techniques was successfully demonstrated. Even though crack formation due to material fatigue limited optical properties of the stretchable electrodes, it aided in guided cellular attachment, which is a beneficial side effect and general challenging topic for biomimetic cell cultivation [187], [188]. However, solution processed graphene/PEDOT:PSS electrodes showed finally only a limited usability for the envisioned electromechanical stimulation platform in stem cell research. Challenges in adhesion promotion between PDMS and the conductive ink film caused major mechanical failure of the structure. Biofunctionalization of patterned electrode surfaces remained a challenge as well, due to the surface expressed material variety in the cell cultivation area.

A novel fabrication procedure for a thin, transparent, piezoelectric composite membrane by surface integration of CNC was introduced and validated. The procedure is based on a combination of CNC thin-film deposition and polymeric composite reinforcement strategies. Uncured PDMS is deposited on a dry crystal film and left to permeate cavities between CNC engulfing the separate crystal structures. The resulting PDMS-CNC composite membrane has an irreversible surface integrated functional CNC thin-film. Spin coated CNC thin-films displayed most promising structural integrity for CNC integration, as they displayed a homogenous CNC layer throughout the surface. However, pre-treatment of CNC solutions allowed variations in CNC thin-film morphology and functionality. The fabricated PDMS-CNC composite membranes displayed measurable piezoelectric activity and could be directly integrated into the mechanical stimulation device for stem cell stimulation. Initial strain analysis revealed no impairment of strain capabilities of PDMS through CNC embedment, as the maximal in-plane strain of the system was retained. Composite membranes also displayed compatibility with biofunctionalization strategies and enhanced the cellular attachment rate compared to a pure

PDMS substrate. The optical transparency of the fabricated composite membrane was sufficient for single-cell analytics and optical microscopy.

However, functionalities of the systems were only studied exemplary throughout this work providing a general tendency suggestion. To verify the obtained results in a quantitative way, extended functional analysis needs to be conducted. Especially, characterizing the electrical response of the PDMS-CNC composite membrane under applied dynamic in-plane strain would be of high importance to define the realistic capabilities of this structure.

Direct electromechanical stimulation of cells through the integration of stretchable electrodes fabricated from conductive polymer in a mechanical stimulation system remains a challenge. Even so, fabricated stretchable electrodes express a general transparency, electrical activity and biocompatibility; Straight-forward electrode integration onto a PDMS surface remains a challenge. The developed system only is functional until a strain of 3.25 %. This is not sufficient in regards of the requirement to regain the mechanical functionality of the introduced mechanical stimulation system However, an equiaxial strain characterization procedure for a graphene/ PEDOT:PSS polymer material was introduced for the first time in this thesis. Stretching tests revealed major performance differences compared to classical uniaxial [78] [94] [90], [138] or biaxial [182]–[184] strain characterization methods. Also, biocompatibility evaluation of Inophene ink was reported for the first time.

A novel manufacturing method for a PDMS-CNC composite membrane is successfully reported in this thesis. The fabricated functional composite membrane fully fulfills the integration requirements to perform as an indirect electro-stimulative extension to the mechanical stimulation device. It is a transparent, stretchable, biocompatible structure with demonstrated piezoelectric sensitivity, which does not alter mechanical or optical properties of the reported mechanical stimulation device. Also it allows single-cell analysis due to its high transparency and supports cellular attachment. Furthermore, the PDMS-CNC composite membrane fabrication procedure can be easily integrated as additional step in the work flow for mechanical stimulation device fabrication. Currently, the applied CNC thin-films consist of randomly oriented CNC. As CNC only express the piezoelectric effect under bending motion in accordance to their piezoelectric coefficient; guiding of crystalline orientation remains a challenge. To enhance the PDMS-CNC composite membrane capabilities and to obtain a uniform electric output from the CNC, crystal alignment procedures are crucial. This will remain a challenge for further work. However, the obtained functional 2D electromechanical stimulation prototype is the first one of its kind. The designed electromechanical stimulation platform is functional without additional electrical controls or wiring, as the integrated piezoelectric CNC thin-film, even though cellulose nanocrystals are randomly oriented, expresses electrical functionality depended on the applied mechanical strain.

6. REFERENCES

[1] F. Gattazzo, A. Urciuolo, and P. Bonaldo, “Extracellular matrix: a dynamic microenvironment for stem cell niche.,” *Biochim. Biophys. Acta*, vol. 1840, no. 8, pp. 2506–19, Aug. 2014.

[2] M. F. Pera and P. P. L. Tam, “Extrinsic regulation of pluripotent stem cells.,” *Nature*, vol. 465, no. 7299, pp. 713–20, Jun. 2010.

[3] Y. Sun, C. S. Chen, and J. Fu, “Forcing stem cells to behave: a biophysical perspective of the cellular microenvironment.,” *Annu. Rev. Biophys.*, vol. 41, pp. 519–42, Jan. 2012.

[4] P.-X. Wan, B.-W. Wang, and Z.-C. Wang, “Importance of the stem cell microenvironment for ophthalmological cell-based therapy.,” *World J. Stem Cells*, vol. 7, no. 2, pp. 448–60, Mar. 2015.

[5] S. D. Eshghi S, “Engineering microenvironments to control stem cell fate and function - PubMed - NCBI,” *Stembook, Cambridge (MA), Harvard Stem Cell Institute*, 2008. [Online]. Available: http://www.ncbi.nlm.nih.gov/pubmed/20614608. [Accessed: 05-Apr-2016].

[6] A. Pavesi, G. Adriani, M. Rasponi, I. K. Zervantonakis, G. B. Fiore, and R. D. Kamm, “Controlled electromechanical cell stimulation on-a-chip.,” *Sci. Rep.*, vol. 5, p. 11800, Jan. 2015.

[7] N. W. S. Kam, E. Jan, and N. A. Kotov, “Electrical stimulation of neural stem cells mediated by humanized carbon nanotube composite made with extracellular matrix protein.,” *Nano Lett.*, vol. 9, no. 1, pp. 273–8, Jan. 2009.

[8] L. G. Griffith and G. Naughton, “Tissue engineering--current challenges and expanding opportunities.,” *Science*, vol. 295, no. 5557, pp. 1009–14, Feb. 2002.

[9] C. Moraes, J.-H. Chen, Y. Sun, and C. A. Simmons, “Microfabricated arrays for high-throughput screening of cellular response to cyclic substrate deformation.,” *Lab Chip*, vol. 10, no. 2, pp. 227–34, Jan. 2010.

[10] L. Huang, P. S. Mathieu, and B. P. Helmke, “A stretching device for high-resolution live-cell imaging.,” *Ann. Biomed. Eng.*, vol. 38, no. 5, pp. 1728–40, May 2010.

[11] L. A. McMahon, A. J. Reid, V. A. Campbell, and P. J. Prendergast, “Regulatory effects of mechanical strain on the chondrogenic differentiation of MSCs in a

collagen-GAG scaffold: experimental and computational analysis.," *Ann. Biomed. Eng.*, vol. 36, no. 2, pp. 185–94, Feb. 2008.

[12] W. W. Ahmed, M. H. Kural, and T. A. Saif, "A novel platform for in situ investigation of cells and tissues under mechanical strain.," *Acta Biomater.*, vol. 6, no. 8, pp. 2979–90, Aug. 2010.

[13] J. Kreutzer, L. Ikonen, J. Hirvonen, M. Pekkanen-Mattila, K. Aalto-Setälä, and P. Kallio, "Pneumatic cell stretching system for cardiac differentiation and culture.," *Med. Eng. Phys.*, vol. 36, no. 4, pp. 496–501, Apr. 2014.

[14] M. Viehrig, S. Tuukkanen, and P. Kallio, "Challenges and Capabilities of Conductive Polymeric Materials for Electromechanical Stimulation of Stem Cells: A Case Study," *Marss 2016*, pp. 1–5, 2016.

[15] M. L. Hammock, A. Chortos, B. C. K. Tee, J. B. H. Tok, and Z. Bao, "25th anniversary article: The evolution of electronic skin (E-Skin): A brief history, design considerations, and recent progress," *Adv. Mater.*, vol. 25, pp. 5997–6038, 2013.

[16] S. J. Benight, C. Wang, J. B. H. Tok, and Z. Bao, "Stretchable and self-healing polymers and devices for electronic skin," *Prog. Polym. Sci.*, vol. 38, no. 12, pp. 1961–1977, Dec. 2013.

[17] A. Blau, A. Murr, S. Wolff, E. Sernagor, P. Medini, G. Iurilli, C. Ziegler, and F. Benfenati, "Flexible, all-polymer microelectrode arrays for the capture of cardiac and neuronal signals.," *Biomaterials*, vol. 32, no. 7, pp. 1778–86, Mar. 2011.

[18] P. Lin, F. Yan, J. Yu, H. L. W. Chan, and M. Yang, "The application of organic electrochemical transistors in cell-based biosensors.," *Adv. Mater.*, vol. 22, no. 33, pp. 3655–60, Sep. 2010.

[19] J. Park, H. K. Kim, and Y. Son, "Glucose biosensor constructed from capped conducting microtubules of PEDOT," *Sensors Actuators B Chem.*, vol. 133, no. 1, pp. 244–250, Jul. 2008.

[20] E. Moczko, G. Istamboulie, C. Calas-Blanchard, R. Rouillon, and T. Noguer, "Biosensor employing screen-printed PEDOT:PSS for sensitive detection of phenolic compounds in water," *J. Polym. Sci. Part A Polym. Chem.*, vol. 50, no. 11, pp. 2286–2292, Jun. 2012.

[21] A. Wisitsoraat, S. Pakapongpan, C. Sriprachuabwong, D. Phokharatkul, P. Sritongkham, T. Lomas, and A. Tuantranont, "Graphene-PEDOT:PSS on screen printed carbon electrode for enzymatic biosensing," *J. Electroanal. Chem.*, vol. 704, pp. 208–213, 2013.

[22] A. Dufresne, “Nanocellulose: a new ageless bionanomaterial,” *Mater. Today*, vol. 16, no. 6, pp. 220–227, Jun. 2013.

[23] Y. Aitomäki and K. Oksman, “Reinforcing efficiency of nanocellulose in polymers,” *React. Funct. Polym.*, vol. 85, pp. 151–156, Dec. 2014.

[24] S. Tuukkanen, S. Rajala, M. Viehrig, and P. Kallio, “Nanocellulose based piezoelectric sensors.” Research Poster, 2016.

[25] N. Lin and A. Dufresne, “Nanocellulose in biomedicine: Current status and future prospect,” *Eur. Polym. J.*, vol. 59, pp. 302–325, Aug. 2014.

[26] L. Csoka, I. C. Hoeger, O. J. Rojas, I. Peszlen, J. J. Pawlak, and P. N. Peralta, “Piezoelectric Effect of Cellulose Nanocrystals Thin Films,” *ACS Macro Lett.*, vol. 1, no. 7, pp. 867–870, Jul. 2012.

[27] B. Frka-Petesic, B. Jean, and L. Heux, “First experimental evidence of a giant permanent electric-dipole moment in cellulose nanocrystals,” *EPL (Europhysics Lett.*, vol. 107, no. 2, p. 28006, Jul. 2014.

[28] L. Li and T. Xie, “Stem Cell Niche: Structure and Function,” *Annu. Rev. Cell Dev. Biol.*, vol. 21, no. 1, pp. 605–631, 2005.

[29] J. Voog and D. L. Jones, “Stem Cells and the Niche: A Dynamic Duo,” *Cell Stem Cell*, vol. 6, no. 2, pp. 103–115, 2010.

[30] F. Guilak, D. M. Cohen, B. T. Estes, J. M. Gimble, W. Liedtke, and C. S. Chen, “Control of Stem Cell Fate by Physical Interactions with the Extracellular Matrix,” *Cell Stem Cell*, vol. 5, no. 1, pp. 17–26, 2009.

[31] H. Ozcelik, M. Hindie, A. Hasan, N. Engin, V. Cell, J. Barthes, H. Özçelik, M. Hindié, A. Ndreu-halili, and N. E. Vrana, “Cell Microenvironment Engineering and Monitoring for Tissue Engineering and Regenerative Medicine : The Citation Accessed Citable Link Cell Microenvironment Engineering and Monitoring for Tissue Engineering and Regenerative Medicine : The Recent Advances,” 2014.

[32] F. Gattazzo, A. Urciuolo, and P. Bonaldo, “Extracellular matrix: A dynamic microenvironment for stem cell niche,” *Biochim. Biophys. Acta - Gen. Subj.*, vol. 1840, no. 8, pp. 2506–2519, 2014.

[33] T. Vazin and D. V. Schaffer, “Engineering strategies to emulate the stem cell niche,” *Trends Biotechnol.*, vol. 28, no. 3, pp. 117–124, 2010.

[34] E. Bellas and C. S. Chen, “Forms, forces, and stem cell fate,” *Curr. Opin. Cell Biol.*, vol. 31, pp. 92–97, 2014.

[35] C. A. Williams and E. B. Lavik, “Engineering the CNS stem cell microenvironment.,” *Regen. Med.*, vol. 4, no. 6, pp. 865–77, 2009.

[36] H. Sauer, G. Rahimi, J. Hescheler, and M. Wartenberg, “Effects of electrical fields on cardiomyocyte differentiation of embryonic stem cells.,” *J. Cell. Biochem.*, vol. 75, no. 4, pp. 710–723, 1999.

[37] M. Radisic, H. Park, H. Shing, T. Consi, F. J. Schoen, R. Langer, L. E. Freed, and G. Vunjak-Novakovic, “Functional assembly of engineered myocardium by electrical stimulation of cardiac myocytes cultured on scaffolds.,” *Proc. Natl. Acad. Sci. U. S. A.*, vol. 101, no. 52, pp. 18129–34, 2004.

[38] I. Kehat, L. Khimovich, O. Caspi, A. Gepstein, R. Shofti, G. Arbel, I. Huber, J. Satin, J. Itskovitz-Eldor, and L. Gepstein, “Electromechanical integration of cardiomyocytes derived from human embryonic stem cells.,” *Nat. Biotechnol.*, vol. 22, no. 10, pp. 1282–1289, 2004.

[39] K. Y. Morgan and L. D. Black, “Mimicking isovolumic contraction with combined electromechanical stimulation improves the development of engineered cardiac constructs.,” *Tissue Eng. Part A*, vol. 20, no. 11–12, pp. 1654–67, Jun. 2014.

[40] E. Ghafar-Zadeh, J. R. Waldeisen, and L. P. Lee, “Engineered approaches to the stem cell microenvironment for cardiac tissue regeneration.,” *Lab Chip*, vol. 11, no. 18, pp. 3031–48, Sep. 2011.

[41] C. Ribeiro, J. Pärssinen, V. Sencadas, V. Correia, S. Miettinen, V. P. Hytönen, and S. Lanceros-Mendez, “Dynamic piezoelectric stimulation enhances osteogenic differentiation of human adipose stem cells,” *J. Biomed. Mater. Res. - Part A*, vol. 103, no. 6, pp. 2172–2175, 2015.

[42] B. M. Rao and P. W. Zandstra, “Culture development for human embryonic stem cell propagation: molecular aspects and challenges.,” *Curr. Opin. Biotechnol.*, vol. 16, no. 5, pp. 568–76, Oct. 2005.

[43] *Animal Cell Culture Methods*. Academic Press, 1998.

[44] ATCC, “ATCC® Animal Cell Culture Guide,” Manassas Vancouver, USA, 2014.

[45] G. Vunjak-Novakovic and D. T. Scadden, “Biomimetic platforms for human stem cell research,” *Cell Stem Cell*, vol. 8, no. 3, pp. 252–261, 2011.

[46] D. A. Lee, M. M. Knight, J. J. Campbell, and D. L. Bader, “Stem cell mechanobiology.,” *J. Cell. Biochem.*, vol. 112, no. 1, pp. 1–9, Jan. 2011.

[47] T. D. Brown, “Techniques for mechanical stimulation of cells in vitro: a review,” *J. Biomech.*, vol. 33, no. 1, pp. 3–14, Jan. 2000.

[48] D. Desmaële, M. Boukallel, and S. Régnier, “Actuation means for the mechanical stimulation of living cells via microelectromechanical systems: A critical review.,” *J. Biomech.*, vol. 44, no. 8, pp. 1433–46, May 2011.

[49] D.-H. Kim, P. K. Wong, J. Park, A. Levchenko, and Y. Sun, “Microengineered platforms for cell mechanobiology.,” *Annu. Rev. Biomed. Eng.*, vol. 11, pp. 203–33, Jan. 2009.

[50] T. A. Desai, “Micro- and nanoscale structures for tissue engineering constructs,” *Med. Eng. Phys.*, vol. 22, no. 9, pp. 595–606, Nov. 2000.

[51] C. Moraes, Y. Sun, and C. A. Simmons, “(Micro)managing the mechanical microenvironment.,” *Integr. Biol. (Camb).*, vol. 3, no. 10, pp. 959–71, Oct. 2011.

[52] W. W. Ahmed, M. H. Kural, and T. A. Saif, “A novel platform for in situ investigation of cells and tissues under mechanical strain.,” *Acta Biomater.*, vol. 6, no. 8, pp. 2979–90, Aug. 2010.

[53] B. J. Pfister, T. P. Weihs, M. Betenbaugh, and G. Bao, “An In Vitro Uniaxial Stretch Model for Axonal Injury,” *Ann. Biomed. Eng.*, vol. 31, no. 5, pp. 589–598, May 2003.

[54] K. Kurpinski, J. Chu, C. Hashi, and S. Li, “Anisotropic mechanosensing by mesenchymal stem cells.,” *Proc. Natl. Acad. Sci. U. S. A.*, vol. 103, no. 44, pp. 16095–100, Oct. 2006.

[55] J. H.-C. Wang, G. Yang, and Z. Li, “Controlling Cell Responses to Cyclic Mechanical Stretching,” *Ann. Biomed. Eng.*, vol. 33, no. 3, pp. 337–342, Jan. 2005.

[56] C. Wan, S. Chung, and R. D. Kamm, “Differentiation of embryonic stem cells into cardiomyocytes in a compliant microfluidic system.,” *Ann. Biomed. Eng.*, vol. 39, no. 6, pp. 1840–7, Jun. 2011.

[57] K. Shimizu, A. Shunori, K. Morimoto, M. Hashida, and S. Konishi, “Development of a biochip with serially connected pneumatic balloons for cell-stretching culture,” *Sensors Actuators B Chem.*, vol. 156, no. 1, pp. 486–493, Aug. 2011.

[58] W. L. Stoppel, D. L. Kaplan, and L. D. Black, “Electrical and mechanical stimulation of cardiac cells and tissue constructs,” *Adv. Drug Deliv. Rev.*, vol. 96, pp. 135–155, 2015.

[59] D. G. Woo, M.-S. Shim, J. S. Park, H. N. Yang, D.-R. Lee, and K.-H. Park, "The effect of electrical stimulation on the differentiation of hESCs adhered onto fibronectin-coated gold nanoparticles.," *Biomaterials*, vol. 30, no. 29, pp. 5631–8, Oct. 2009.

[60] M. Zhao, H. Bai, E. Wang, J. V Forrester, and C. D. McCaig, "Electrical stimulation directly induces pre-angiogenic responses in vascular endothelial cells by signaling through VEGF receptors.," *J. Cell Sci.*, vol. 117, no. Pt 3, pp. 397–405, 2004.

[61] S. Rangarajan, L. Madden, and N. Bursac, "Use of flow, electrical, and mechanical stimulation to promote engineering of striated muscles," *Ann. Biomed. Eng.*, vol. 42, no. 7, pp. 1391–1405, 2014.

[62] M. Yamada, K. Tanemura, S. Okada, A. Iwanami, M. Nakamura, H. Mizuno, M. Ozawa, R. Ohyama-Goto, N. Kitamura, M. Kawano, K. Tan-Takeuchi, C. Ohtsuka, A. Miyawaki, A. Takashima, M. Ogawa, Y. Toyama, H. Okano, and T. Kondo, "Electrical stimulation modulates fate determination of differentiating embryonic stem cells.," *Stem Cells*, vol. 25, no. 3, pp. 562–570, 2007.

[63] S. Karumbayaram, B. G. Novitch, M. Patterson, J. A. Umbach, L. Richter, A. Lindgren, A. E. Conway, A. T. Clark, S. A. Goldman, K. Plath, M. Wiedau-Pazos, H. I. Kornblum, and W. E. Lowry, "Directed differentiation of human-induced pluripotent stem cells generates active motor neurons," *Stem Cells*, vol. 27, no. 4, pp. 806–811, 2009.

[64] N. Kam, E. Jan, and N. Kotov, "Electrical stimulation of neural stem cells mediated by humanized carbon nanotube composite made with extracellular matrix protein," *Nano Lett.*, no. 2, 2008.

[65] C. H. Chen, K. I. Sereti, B. M. Wu, and R. Ardehali, "Translational aspects of cardiac cell therapy," *J. Cell. Mol. Med.*, vol. 19, no. 8, pp. 1757–1772, 2015.

[66] J. L. Young and A. J. Engler, "Hydrogels with time-dependent material properties enhance cardiomyocyte differentiation in vitro.," *Biomaterials*, vol. 32, no. 4, pp. 1002–9, Feb. 2011.

[67] G. Vunjak-Novakovic, S. Bhatia, C. Chen, and K. Hirschi, "HeLiVa platform: integrated heart-liver-vascular systems for drug testing in human health and disease.," *Stem Cell Res. Ther.*, vol. 4 Suppl 1, no. 1, p. S8, Jan. 2013.

[68] J. Ge, L. Sun, F. R. Zhang, Y. Zhang, L. A. Shi, H. Y. Zhao, H. W. Zhu, H. L. Jiang, and S. H. Yu, "A Stretchable Electronic Fabric Artificial Skin with Pressure-, Lateral Strain-, and Flexion-Sensitive Properties," *Adv. Mater.*, pp.

722–728, 2015.

[69] M. L. Hammock, A. Chortos, B. C.-K. Tee, J. B.-H. Tok, and Z. Bao, “25th anniversary article: The evolution of electronic skin (e-skin): a brief history, design considerations, and recent progress.,” *Adv. Mater.*, vol. 25, no. 42, pp. 5997–6038, Nov. 2013.

[70] T. Someya, Ed., *Stretchable Electronics*. Weinheim, Germany: Wiley-VCH Verlag GmbH & Co. KGaA, 2012.

[71] R. D. Mehlenbacher, T. J. McDonough, M. Grechko, M.-Y. Wu, M. S. Arnold, and M. T. Zanni, “Energy transfer pathways in semiconducting carbon nanotubes revealed using two-dimensional white-light spectroscopy.,” *Nat. Commun.*, vol. 6, p. 6732, Jan. 2015.

[72] I. Jeon, T. Chiba, C. Delacou, Y. Guo, A. Kaskela, O. Reynaud, E. I. Kauppinen, S. Maruyama, and Y. Matsuo, “Single-Walled Carbon Nanotube Film as Electrode in Indium-Free Planar Heterojunction Perovskite Solar Cells: Investigation of Electron-Blocking Layers and Dopants.,” *Nano Lett.*, vol. 15, no. 10, pp. 6665–71, Oct. 2015.

[73] G. Gruner, “Carbon nanotube films for transparent and plastic electronics,” *J. Mater. Chem.*, vol. 16, no. 35, p. 3533, Sep. 2006.

[74] E. H. Hwang, S. Adam, and S. Das Sarma, “Carrier Transport in Two-Dimensional Graphene Layers,” *Phys. Rev. Lett.*, vol. 98, no. 18, p. 186806, May 2007.

[75] *Graphene: An Introduction to the Fundamentals and Industrial Applications*. Wiley, 2015.

[76] A. Mata, A. J. Fleischman, and S. Roy, “Characterization of polydimethylsiloxane (PDMS) properties for biomedical micro/nanosystems.,” *Biomed. Microdevices*, vol. 7, no. 4, pp. 281–93, Dec. 2005.

[77] T. Lu, L. Finkenauer, J. Wissman, and C. Majidi, “Rapid prototyping for soft-matter electronics,” *Adv. Funct. Mater.*, vol. 24, no. 22, pp. 3351–3356, 2014.

[78] D. J. Lipomi, J. A. Lee, M. Vosgueritchian, B. C.-K. Tee, J. A. Bolander, and Z. Bao, “Electronic Properties of Transparent Conductive Films of PEDOT:PSS on Stretchable Substrates,” *Chem. Mater.*, vol. 24, no. 2, pp. 373–382, Jan. 2012.

[79] B. Charlot, G. Sassine, A. Garraud, B. Sorli, A. Giani, and P. Combette, “Micropatterning PEDOT:PSS layers,” *Microsyst. Technol.*, vol. 19, no. 6, pp. 895–903, 2013.

[80] B. D. Malhotra, A. Chaubey, and S. P. Singh, “Prospects of conducting polymers in biosensors,” *Anal. Chim. Acta*, vol. 578, no. 1, pp. 59–74, 2006.

[81] U. Lange, N. V. Roznyatovskaya, and V. M. Mirsky, “Conducting polymers in chemical sensors and arrays,” *Anal. Chim. Acta*, vol. 614, no. 1, pp. 1–26, 2008.

[82] B. Adhikari and S. Majumdar, “Polymers in sensor applications,” *Prog. Polym. Sci.*, vol. 29, no. 7, pp. 699–766, 2004.

[83] T. Ahuja, I. A. Mir, D. Kumar, and Rajesh, “Biomolecular immobilization on conducting polymers for biosensing applications,” *Biomaterials*, vol. 28, no. 5, pp. 791–805, 2007.

[84] N. K. Guimard, N. Gomez, and C. E. Schmidt, “Conducting polymers in biomedical engineering,” *Prog. Polym. Sci.*, vol. 32, no. 8–9, pp. 876–921, 2007.

[85] C. Paper and I. Branch, “Application of Conducting Polymers As,” vol. 17, no. October, pp. 1–2, 2015.

[86] O. Berezhetska, B. Liberelle, G. De Crescenzo, and F. Cicoira, “A simple approach for protein covalent grafting on conducting polymer films,” *J. Mater. Chem. B*, vol. 3, no. 25, pp. 5087–5094, Jun. 2015.

[87] N. Aydemir, J. Malmström, and J. Travas-Sejdic, “Conducting polymer based electrochemical biosensors.,” *Phys. Chem. Chem. Phys.*, vol. 18, no. 12, pp. 8264–77, Mar. 2016.

[88] H. Yoon, “Current Trends in Sensors Based on Conducting Polymer Nanomaterials,” *Nanomaterials*, vol. 3, no. 3, pp. 524–549, 2013.

[89] T. Isoniemi, S. Tuukkanen, and D. Cameron, “Measuring optical anisotropy in poly (3, 4-ethylene dioxythiophene): poly (styrene sulfonate) films with added graphene,” *Org. …*, 2015.

[90] U. Lang, N. Naujoks, and J. Dual, “Mechanical characterization of PEDOT:PSS thin films,” *Synth. Met.*, vol. 159, no. 5–6, pp. 473–479, Mar. 2009.

[91] J. R. Potts, D. R. Dreyer, C. W. Bielawski, and R. S. Ruoff, “Graphene-based polymer nanocomposites,” *Polymer (Guildf).*, vol. 52, no. 1, pp. 5–25, Jan. 2011.

[92] T. Vuorinen, M. Zakrzewski, S. Rajala, D. Lupo, J. Vanhala, K. Palovuori, and S. Tuukkanen, “Printable, Transparent, and Flexible Touch Panels Working in Sunlight and Moist Environments,” *Adv. Funct. Mater.*, vol. 24, no. 40, pp. 6340–6347, Oct. 2014.

[93] S. Rajala, S. Tuukkanen, and J. Halttunen, “Characteristics of Piezoelectric

Polymer Film Sensors With Solution-Processable Graphene-Based Electrode Materials," *IEEE Sens. J.*, vol. 15, no. 6, pp. 3102–3109, Jun. 2015.

[94] S. N. K. Rajala, M. Mettanen, and S. Tuukkanen, "Structural and Electrical Characterization of Solution-Processed Electrodes for Piezoelectric Polymer Film Sensors," *IEEE Sens. J.*, vol. 16, no. 6, pp. 1692–1699, Mar. 2016.

[95] Y. Habibi, L. A. Lucia, and O. J. Rojas, "Cellulose Nanocrystals : Chemistry , Self-Assembly , and Applications," vol. d, pp. 3479–3500, 2010.

[96] J. R. Capadona, O. Van Den Berg, L. A. Capadona, M. Schroeter, S. J. Rowan, D. J. Tyler, and C. Weder, "A versatile approach for the processing of polymer nanocomposites with self-assembled nanofibre templates.," *Nat. Nanotechnol.*, vol. 2, no. 12, pp. 765–9, Dec. 2007.

[97] A. Samzadeh-Kermani and N. Esfandiary, "Synthesis and Characterization of New Biodegradable Chitosan/Polyvinyl Alcohol/Cellulose Nanocomposite," *Adv. Nanoparticles*, vol. 05, no. 01, pp. 18–26, Feb. 2016.

[98] Y. Lu, L. Weng, and X. Cao, "Biocomposites of plasticized starch reinforced with cellulose crystallites from cottonseed linter.," *Macromol. Biosci.*, vol. 5, no. 11, pp. 1101–7, Nov. 2005.

[99] S. Kalia, A. Dufresne, B. M. Cherian, B. S. Kaith, L. Avérous, J. Njuguna, and E. Nassiopoulos, "Cellulose-based bio- and nanocomposites: A review," *Int. J. Polym. Sci.*, vol. 2011, 2011.

[100] A. Dufresne, "Processing of polymer nanocomposites reinforced with polysaccharide nanocrystals," *Molecules*, vol. 15, no. 6, pp. 4111–4128, 2010.

[101] K. Y. Lee, Y. Aitom??ki, L. A. Berglund, K. Oksman, and A. Bismarck, "On the use of nanocellulose as reinforcement in polymer matrix composites," *Compos. Sci. Technol.*, vol. 105, pp. 15–27, 2014.

[102] Y. Zheng, J. Monty, and R. J. Linhardt, "Polysaccharide-based nanocomposites and their applications.," *Carbohydr. Res.*, vol. 405, pp. 23–32, Mar. 2015.

[103] H. Y. Yu, R. Chen, G. Y. Chen, L. Liu, X. G. Yang, and J. M. Yao, "Silylation of cellulose nanocrystals and their reinforcement of commercial silicone rubber," *J. Nanoparticle Res.*, vol. 17, no. 9, pp. 1–13, 2015.

[104] J. Yang, J. J. Zhao, F. Xu, and R. C. Sun, "Revealing strong nanocomposite hydrogels reinforced by cellulose nanocrystals: Insight into morphologies and interactions," *ACS Appl. Mater. Interfaces*, vol. 5, no. 24, pp. 12960–12967, 2013.

[105] V. Jankauskaite, B. Abzalbelkuy, A. Lisauskaite, I. Procyecevas, E. Fataraite, and A. Vitkauskiene, “Silicone rubber and microcrystalline cellulose composites with antimicrobial properties,” *Mater. Sci.*, vol. 20, no. 1, pp. 42–49, 2014.

[106] D. S. Kim, S. M. Jung, G. H. Yoon, H. C. Lee, and H. S. Shin, “Development of a complex bone tissue culture system based on cellulose nanowhisker mechanical strain,” *Colloids Surfaces B Biointerfaces*, vol. 123, pp. 838–844, 2014.

[107] Z. Hu, E. D. Cranston, R. Ng, and R. Pelton, “Tuning cellulose nanocrystal gelation with polysaccharides and surfactants.,” *Langmuir*, vol. 30, no. 10, pp. 2684–92, 2014.

[108] K. A. Mahmoud, K. B. Male, S. Hrapovic, and J. H. T. Luong, “Cellulose nanocrystal/gold nanoparticle composite as a matrix for enzyme immobilization,” *ACS Appl. Mater. Interfaces*, vol. 1, no. 7, pp. 1383–1386, 2009.

[109] S. Arola, *Biochemical modifi cation and functionalization of nanocellulose surface*. 2015.

[110] S. Rajala, T. Siponkoski, E. Sarlin, M. Mettänen, Marja Vuoriluoto, A. Pammo, J. Juuti, O. Rojas, and S. Franssila, Sami Tuukkanen, “Cellulose nanofibril film as a piezoelectric sensor material,” *ACS Appl. Mater. Interfaces*, 2016.

[111] J. Araki and S. Kuga, “Effect of Trace Electrolyte on Liquid Crystal Type of Cellulose Microcrystals,” *Langmuir*, vol. 17, no. 15, pp. 4493–4496, Jul. 2001.

[112] X. Wu, R. J. Moon, and A. Martini, “Crystalline cellulose elastic modulus predicted by atomistic models of uniform deformation and nanoscale indentation,” *Cellulose*, vol. 20, no. 1, pp. 43–55, Nov. 2012.

[113] J. F. Nye, “The Physical Properties of Crystals,” Jan. 1990.

[114] E. Fukada, “Piezoelectricity of Wood,” *J. Phys. Soc. Japan*, vol. 10, no. 2, pp. 149–154, Feb. 1955.

[115] S. Rajala, M. Vuoriluoto, O. J. Rojas, S. Franssila, and S. Tuukkanen, “Piezoelectric sensitivity measurements of cellulose nanofibril sensors,” in *IMEKO XXI World Congress, Proceedings, August 30 - September 4, 2015, Prague, Czech Republic*, 2015.

[116] M. S. Inc., “Piezo film sensors,” *Technical manual*, 2016. .

[117] G. Eberle, H. Schmidt, and W. Eisenmenger, “Piezoelectric polymer electrets,” *IEEE Trans. Dielectr. Electr. Insul.*, vol. 3, no. 5, pp. 624–646, 1996.

[118] Y. Li, H. Ren, and A. J. Ragauskas, “Rigid polyurethane foam reinforced with

cellulose whiskers: Synthesis and characterization," *Nano-Micro Lett.*, vol. 2, no. 2, pp. 89–94, May 2010.

[119] Y. Wang, X. Cao, and L. Zhang, "Effects of cellulose whiskers on properties of soy protein thermoplastics.," *Macromol. Biosci.*, vol. 6, no. 7, pp. 524–31, Jul. 2006.

[120] D. Dubief, E. Samain, and A. Dufresne, "Polysaccharide Microcrystals Reinforced Amorphous Poly(β-hydroxyoctanoate) Nanocomposite Materials," *Macromolecules*, vol. 32, no. 18, pp. 5765–5771, Sep. 1999.

[121] R. Z. Khoo, H. Ismail, and W. S. Chow, "Thermal and Morphological Properties of Poly (Lactic Acid)/Nanocellulose Nanocomposites," *Procedia Chem.*, vol. 19, pp. 788–794, 2016.

[122] D. Bondeson and K. Oksman, "Polylactic acid/cellulose whisker nanocomposites modified by polyvinyl alcohol," *Compos. Part A Appl. Sci. Manuf.*, vol. 38, no. 12, pp. 2486–2492, Dec. 2007.

[123] M. Eriksson, S. M. Notley, and L. Wågberg, "Cellulose thin films: Degree of cellulose ordering and its influence on adhesion," *Biomacromolecules*, vol. 8, no. 3, pp. 912–919, 2007.

[124] M. Eita, H. Arwin, H. Granberg, and L. Wågberg, "Addition of silica nanoparticles to tailor the mechanical properties of nanofibrillated cellulose thin films," *J. Colloid Interface Sci.*, vol. 363, no. 2, pp. 566–572, 2011.

[125] C. Salas, T. Nypelö, C. Rodriguez-Abreu, C. Carrillo, and O. J. Rojas, "Nanocellulose properties and applications in colloids and interfaces," *Curr. Opin. Colloid Interface Sci.*, vol. 19, no. 5, pp. 383–396, 2014.

[126] D. J. Gardner, G. S. Oporto, R. Mills, and M. A. S. Azizi Samir, "Adhesion and surface issues in cellulose and nanocellulose," *J. Adhes. Sci. Technol.*, vol. 22, no. 5–6, pp. 545–567, 2008.

[127] R. I. Freshney, *Culture of Animal Cells: A Manual of Basic Technique and Specialized Applications*. Wiley, 2015.

[128] J. Schindelin, I. Arganda-Carreras, E. Frise, V. Kaynig, M. Longair, T. Pietzsch, S. Preibisch, C. Rueden, S. Saalfeld, B. Schmid, J.-Y. Tinevez, D. J. White, V. Hartenstein, K. Eliceiri, P. Tomancak, and A. Cardona, "Fiji: an open-source platform for biological-image analysis.," *Nat. Methods*, vol. 9, no. 7, pp. 676–82, Jul. 2012.

[129] I. F. Sbalzarini and P. Koumoutsakos, "Feature point tracking and trajectory

analysis for video imaging in cell biology.," *J Struct Biol*, vol. 151, no. 2, pp. 182–95, 2005.

[130] M. Viehrig, S. Tuukkanen, and P. Kallio, "Challenges and Capabilities of Conductive Polymeric Materials for Electromechanical Stimulation of Stem Cells: A Case Study," in *MARSS 2016*, 2016.

[131] L. Innophene Co., "MSDS P3014-Safety Data Sheet." pp. 1–5, 2012.

[132] T. Lu, L. Finkenauer, J. Wissman, and C. Majidi, "Rapid Prototyping for Soft-Matter Electronics," *Adv. Funct. Mater.*, vol. 24, no. 22, pp. 3351–3356, Jun. 2014.

[133] D. J. Lipomi, J. a Lee, M. Vosgueritchian, B. C. Tee, J. a Bolander, and Z. Bao, "on Stretchable Substrates," 2012.

[134] B. Charlot, G. Sassine, A. Garraud, B. Sorli, A. Giani, and P. Combette, "Micropatterning PEDOT:PSS layers," *Microsyst. Technol.*, vol. 19, no. 6, pp. 895–903, Nov. 2012.

[135] B. Wei, J. Liu, L. Ouyang, C.-C. Kuo, and D. C. Martin, "Significant enhancement of PEDOT thin film adhesion to inorganic solid substrates with EDOT-acid.," *ACS Appl. Mater. Interfaces*, vol. 7, no. 28, pp. 15388–94, Jul. 2015.

[136] K. Fong Lei, *Microfluidics in Detection Science*. Cambridge: Royal Society of Chemistry, 2014.

[137] K. Wasa, M. Kitabatake, and H. Adachi, *Thin film materials technology: sputtering of control compound materials*. Springer Science & Business Media, 2004.

[138] S. Tuukkanen, M. Hoikkanen, M. Poikelispää, M. Honkanen, T. Vuorinen, M. Kakkonen, J. Vuorinen, and D. Lupo, "Stretching of solution processed carbon nanotube and graphene nanocomposite films on rubber substrates," *Synth. Met.*, vol. 191, pp. 28–35, 2014.

[139] M. J. Lee, N. Y. Lee, J. R. Lim, J. B. Kim, M. Kim, H. K. Baik, and Y. S. Kim, "Antiadhesion Surface Treatments of Molds for High-Resolution Unconventional Lithography," *Adv. Mater.*, vol. 18, no. 23, pp. 3115–3119, Dec. 2006.

[140] J. Kim, M. Kim, M. J. Lee, J. S. Lee, K. Shin, and Y. S. Kim, "Low-Cost Fabrication of Transparent Hard Replica Molds for Imprinting Lithography," *Adv. Mater.*, vol. 21, no. 40, pp. 4050–4053, Oct. 2009.

[141] U. S. A. D3359-97, “Standard Test Methods for Measuring Adhesion by Tape Test.,” 1997.

[142] S. M. Wolniak, “Principles of Light Microscopy,” *Teaching Interest, University of Maryland*, 2004. [Online]. Available: http://www.life.umd.edu/cbmg/faculty/wolniak/wolniakmicro.html. [Accessed: 11-May-2016].

[143] R. Rottenfusser, E. E. Wilson, and M. W. Davidson, “Microscopy Basics | Numerical Aperture and Resolution,” *Carl Zeiss Microscopy Online Campus*, 2015. [Online]. Available: http://zeiss-campus.magnet.fsu.edu/articles/basics/resolution.html. [Accessed: 11-May-2016].

[144] M. E. Dailey, A. Khodjakov, C. L. Rieder, M. Platani, J. R. Swedlow, P. D. Andrews, Y. Wang, J. C. Waters, N. S. Claxton, S. G. Olenych, J. D. Griffin, and M. W. Davidson, “Optical System and Detector Requirements for Live-Cell Imaging,” *Nikon MicroscopyU*, 2015. [Online]. Available: http://www.microscopyu.com/articles/livecellimaging/imagingsystems.html. [Accessed: 11-May-2016].

[145] W. Mai, “Fundamental Theory of Atomic Force Microscopy,” 2000. [Online]. Available: http://www.nanoscience.gatech.edu/zlwang/research/afm.html. [Accessed: 11-May-2016].

[146] Park Systems, “AFM Principle - How AFM Works | Park Atomic Force Microscope,” 2015. [Online]. Available: http://www.parkafm.com/index.php/medias/nano-academy/how-afm-works. [Accessed: 11-May-2016].

[147] J. P. F. Lagerwall, C. Schütz, M. Salajkova, J. Noh, J. Hyun Park, G. Scalia, and L. Bergström, “Cellulose nanocrystal-based materials: from liquid crystal self-assembly and glass formation to multifunctional thin films,” *NPG Asia Mater.*, vol. 6, no. 1, p. e80, 2014.

[148] M. P. Pileni, “Nanocrystal Self-Assemblies: Fabrication and Collective Properties,” *J. Phys. Chem. B*, vol. 105, no. 17, pp. 3358–3371, 2001.

[149] a Pizzoferrato, G. Ciapetti, S. Stea, E. Cenni, C. R. Arciola, D. Granchi, and L. Savarino, “Cell culture methods for testing biocompatibility.,” *Clin. Mater.*, vol. 15, no. 3, pp. 173–190, Jan. 1994.

[150] C. T. Hanks, J. C. Wataha, and Z. Sun, “In vitro models of biocompatibility: a review.,” *Dent. Mater.*, vol. 12, no. 3, pp. 186–93, May 1996.

[151] H. J. Johnson, S. J. Northup, P. A. Seagraves, P. J. Garvin, and R. F. Wallin, “Biocompatibility test procedures for materials evaluation in vitro. I. Comparative test system sensitivity.,” *J. Biomed. Mater. Res.*, vol. 17, no. 4, pp. 571–86, Jul. 1983.

[152] H. J. Johnson, S. J. Northup, P. A. Seagraves, M. Atallah, P. J. Garvin, L. Lin, and T. D. Darby, “Biocompatibility test procedures for materials evaluation in vitro. II. Objective methods of toxicity assessment.,” *J. Biomed. Mater. Res.*, vol. 19, no. 5, pp. 489–508, Jan. .

[153] H. Ju, X. Zhang, and J. Wang, *NanoBiosensing*. New York, NY: Springer New York, 2011.

[154] “Wiley: Biofunctionalization of Nanomaterials - Challa S. S. R. Kumar.” [Online]. Available: http://eu.wiley.com/WileyCDA/WileyTitle/productCd-3527313818.html. [Accessed: 11-May-2016].

[155] M. Tallawi, E. Rosellini, N. Barbani, M. G. Cascone, R. Rai, G. Saint-Pierre, and A. R. Boccaccini, “Strategies for the chemical and biological functionalization of scaffolds for cardiac tissue engineering: a review.,” *J. R. Soc. Interface*, vol. 12, no. 108, p. 20150254, Jul. 2015.

[156] D. Khatayevich, M. Gungormus, H. Yazici, C. So, S. Cetinel, H. Ma, A. Jen, C. Tamerler, and M. Sarikaya, “Biofunctionalization of materials for implants using engineered peptides.,” *Acta Biomater.*, vol. 6, no. 12, pp. 4634–41, Dec. 2010.

[157] A. M. Debela, M. Ortiz, V. Beni, S. Thorimbert, D. Lesage, R. B. Cole, C. K. O’Sullivan, and B. Hasenknopf, “Biofunctionalization of Polyoxometalates with DNA Primers, Their Use in the Polymerase Chain Reaction (PCR) and Electrochemical Detection of PCR Products.,” *Chemistry*, vol. 21, no. 49, pp. 17721–7, Dec. 2015.

[158] M. Palma, J. J. Abramson, A. A. Gorodetsky, C. Nuckolls, M. P. Sheetz, S. J. Wind, and J. Hone, “Controlled confinement of DNA at the nanoscale: nanofabrication and surface bio-functionalization.,” *Methods Mol. Biol.*, vol. 749, pp. 169–85, Jan. 2011.

[159] R. van Vught, R. J. Pieters, and E. Breukink, “Site-specific functionalization of proteins and their applications to therapeutic antibodies.,” *Comput. Struct. Biotechnol. J.*, vol. 9, p. e201402001, Jan. 2014.

[160] P. Jain, S. Varshney, and S. Srivastava, “Site-specific functionalization for chemical speciation of Cr(III) and Cr(VI) using polyaniline impregnated nanocellulose composite: equilibrium, kinetic, and thermodynamic modeling,”

Appl. Water Sci., Oct. 2015.

[161] S. Puertas, P. Batalla, M. Moros, E. Polo, P. Del Pino, J. M. Guisan, V. Grazú, and J. M. de la Fuente, "Taking advantage of unspecific interactions to produce highly active magnetic nanoparticle-antibody conjugates.," *ACS Nano*, vol. 5, no. 6, pp. 4521–8, Jun. 2011.

[162] X. Punet, R. Mauchauffé, M. I. Giannotti, J. C. Rodríguez-Cabello, F. Sanz, E. Engel, M. A. Mateos-Timoneda, and J. A. Planell, "Enhanced cell-material interactions through the biofunctionalization of polymeric surfaces with engineered peptides.," *Biomacromolecules*, vol. 14, no. 8, pp. 2690–702, Aug. 2013.

[163] A. Gelmi, M. K. Ljunggren, M. Rafat, and E. W. H. Jager, "Influence of conductive polymer doping on the viability of cardiac progenitor cells," *J. Mater. Chem. B*, vol. 2, no. 24, p. 3860, 2014.

[164] B. Alberts, A. Johnson, J. Lewis, M. Raff, K. Roberts, and P. Walter, "Fibroblasts and Their Transformations: The Connective-Tissue Cell Family." Garland Science, 2002.

[165] "Fibroblast Cells General Information and Resources." [Online]. Available: http://www.fibroblast.org/. [Accessed: 11-May-2016].

[166] "Fibroblast | Anatomy," *Britannica*. 2015.

[167] M. A. Carlson, L. M. Smith, C. M. Cordes, J. Chao, and J. D. Eudy, "Attachment-regulated signaling networks in the fibroblast-populated 3D collagen matrix.," *Sci. Rep.*, vol. 3, p. 1880, Jan. 2013.

[168] M. Amit, V. Margulets, H. Segev, K. Shariki, I. Laevsky, R. Coleman, and J. Itskovitz-Eldor, "Human feeder layers for human embryonic stem cells.," *Biol. Reprod.*, vol. 68, no. 6, pp. 2150–6, Jun. 2003.

[169] A. Choo, J. Padmanabhan, A. Chin, W. J. Fong, and S. K. W. Oh, "Immortalized feeders for the scale-up of human embryonic stem cells in feeder and feeder-free conditions.," *J. Biotechnol.*, vol. 122, no. 1, pp. 130–41, Mar. 2006.

[170] C. Unger, S. Gao, M. Cohen, M. Jaconi, R. Bergstrom, F. Holm, A. Galan, E. Sanchez, O. Irion, J. B. Dubuisson, M. Giry-Laterriere, P. Salmon, C. Simon, O. Hovatta, and A. Feki, "Immortalized human skin fibroblast feeder cells support growth and maintenance of both human embryonic and induced pluripotent stem cells.," *Hum. Reprod.*, vol. 24, no. 10, pp. 2567–81, Oct. 2009.

[171] K. Takahashi, K. Tanabe, M. Ohnuki, M. Narita, T. Ichisaka, K. Tomoda, and S.

Yamanaka, “Induction of pluripotent stem cells from adult human fibroblasts by defined factors.,” *Cell*, vol. 131, no. 5, pp. 861–72, Nov. 2007.

[172] Y. Shamis, K. J. Hewitt, M. W. Carlson, M. Margvelashvilli, S. Dong, C. K. Kuo, L. Daheron, C. Egles, and J. A. Garlick, “Fibroblasts derived from human embryonic stem cells direct development and repair of 3D human skin equivalents.,” *Stem Cell Res. Ther.*, vol. 2, no. 1, p. 10, Jan. 2011.

[173] J.-H. Moon, J. S. Heo, J. S. Kim, E. K. Jun, J. H. Lee, A. Kim, J. Kim, K. Y. Whang, Y.-K. Kang, S. Yeo, H.-J. Lim, D. W. Han, D.-W. Kim, S. Oh, B. S. Yoon, H. R. Schöler, and S. You, “Reprogramming fibroblasts into induced pluripotent stem cells with Bmi1.,” *Cell Res.*, vol. 21, no. 9, pp. 1305–15, Sep. 2011.

[174] B. Saad, O. M. Keiser, M. Welti, G. K. Uhlschmid, P. Neuenschwander, and U. W. Suter, “Multiblock copolyesters as biomaterials: in vitro biocompatibility testing,” *J. Mater. Sci. Mater. Med.*, vol. 8, no. 8, pp. 497–505.

[175] R. Villa, C. R. Ortiz, S. Tapia, G. Gonzalez, E. Trillo, K. M. Garza, S. W. Stafford, and L. E. Murr, “In Vitro Biocompatibility Studies of Fibroblast Cells on Ti-Ta Alloys.,” *Mater. Trans.*, vol. 43, no. 12, pp. 2991–2994, Sep. 2002.

[176] A. A. Ignatius and L. E. Claes, “In vitro biocompatibility of bioresorbable polymers: poly(L, DL-lactide) and poly(L-lactide-co-glycolide),” *Biomaterials*, vol. 17, no. 8, pp. 831–839, Jan. 1996.

[177] C. Morrison, R. Macnair, C. MacDonald, A. Wykman, I. Goldie, and M. H. Grant, “In vitro biocompatibility testing of polymers for orthopaedic implants using cultured fibroblasts and osteoblasts,” *Biomaterials*, vol. 16, no. 13, pp. 987–992, Sep. 1995.

[178] W. Xu, H. Baribault, and E. D. Adamson, “Vinculin knockout results in heart and brain defects during embryonic development,” *Development*, no. 125/2, Jan. 1998.

[179] J. P. Mather and P. E. Roberts, *Introduction to Cell and Tissue Culture: Theory and Technique*. Springer Science & Business Media, 2007.

[180] K. Kono, N. Takada, S. Yasuda, R. Sawada, S. Niimi, A. Matsuyama, and Y. Sato, “Characterization of the cell growth analysis for detection of immortal cellular impurities in human mesenchymal stem cells.,” *Biologicals*, vol. 43, no. 2, pp. 146–9, Mar. 2015.

[181] C. Dang, T. A. Gilewski, A. Surbone, and L. Norton, “Growth Curve Analysis.” BC Decker, 2003.

[182] S. Savagatrup, A. S. Makaram, D. J. Burke, and D. J. Lipomi, “Mechanical Properties of Conjugated Polymers and Polymer-Fullerene Composites as a Function of Molecular Structure,” *Adv. Funct. Mater.*, vol. 24, no. 8, pp. 1169–1181, Feb. 2014.

[183] K. Xie and B. Wei, “Materials and structures for stretchable energy storage and conversion devices.,” *Adv. Mater.*, vol. 26, no. 22, pp. 3592–617, Jun. 2014.

[184] D. J. Gundlach, T. N. Jackson, D. G. Schlom, and S. F. Nelson, “Solvent-induced phase transition in thermally evaporated pentacene films,” *Appl. Phys. Lett.*, vol. 74, no. 22, p. 3302, May 1999.

[185] M. Marzocchi, I. Gualandi, M. Calienni, I. Zironi, E. Scavetta, G. Castellani, and B. Fraboni, “Physical and Electrochemical Properties of PEDOT:PSS as a Tool for Controlling Cell Growth,” *ACS Appl. Mater. Interfaces*, vol. 7, no. 32, pp. 17993–18003, 2015.

[186] S. J. Eichhorn, “Stiff as a board: Perspectives on the crystalline modulus of cellulose,” *ACS Macro Lett.*, vol. 1, no. 11, pp. 1237–1239, 2012.

[187] H. Wang, W. Ip, R. Boissy, and E. S. Grood, “Cell orientation response to cyclically deformed substrates: Experimental validation of a cell model,” *J. Biomech.*, vol. 28, no. 12, pp. 1543–1552, Dec. 1995.

[188] D. Strutt, “Organ shape: controlling oriented cell division.,” *Curr. Biol.*, vol. 15, no. 18, pp. R758–9, Sep. 2005.

APPENDIX A: DUMBBELL CHANNEL ELECTRODE STRETCHING

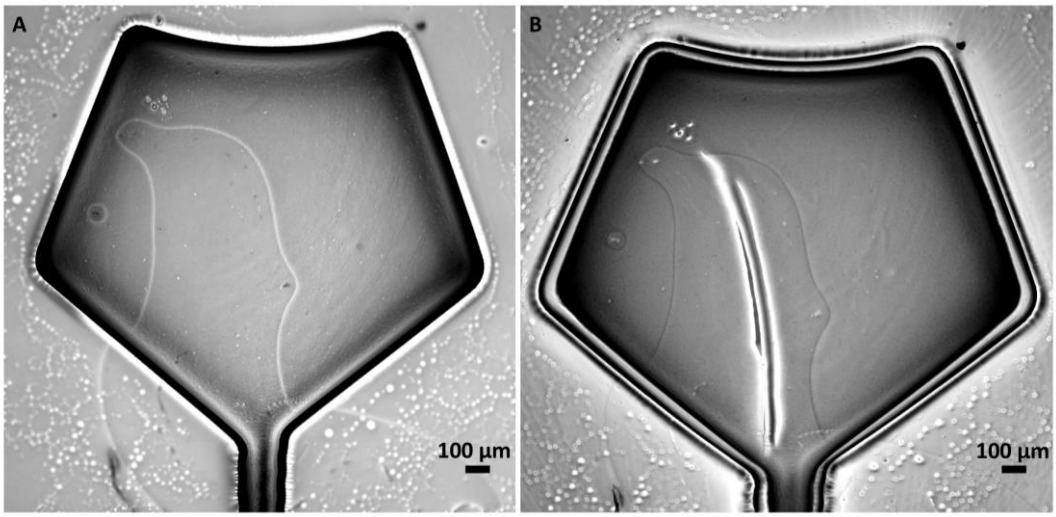

Figure 1. *Inner connection pad of a dumbbell channel electrode filled with Innophene. Electrode morphology changes between 0 % (A) and 10 % (B) applied strain. Edge delamination and material cracking are apparent at 10 % applied strain (B).*

APPENDIX B: PDMS-CNC COMPOSITE MEMBRANE ADHESION TEST

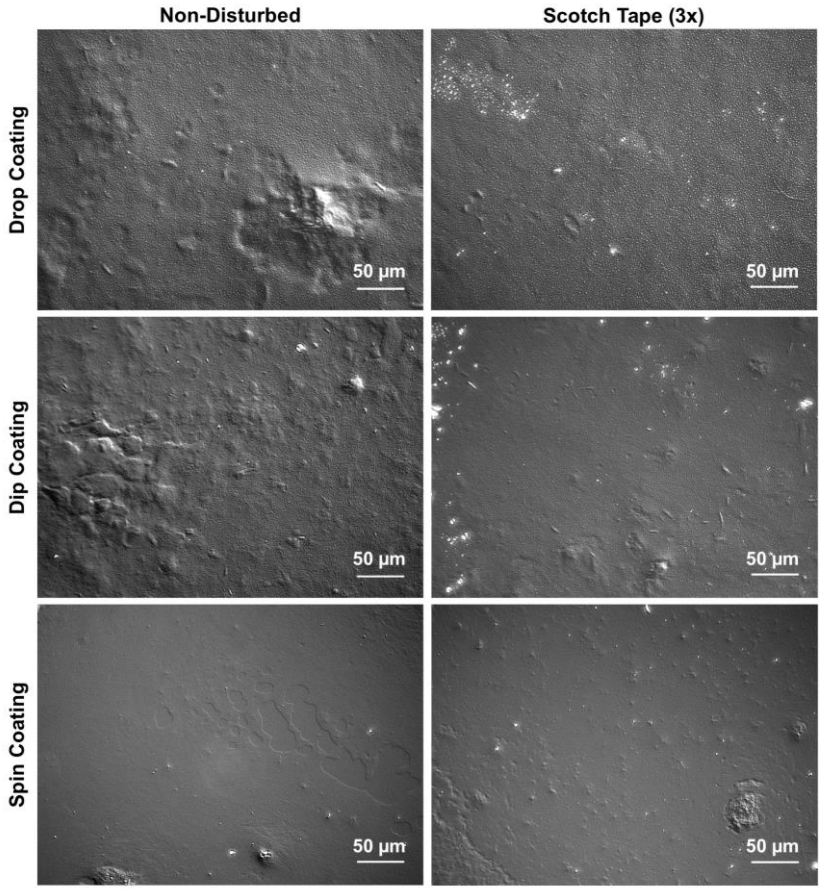

Figure 2. *Adhesion testing of PDMS-CNC composite membranes prepared by various deposition methods.*